

**EVALUATION OF HIGH TEMPERATURE  
BOILER TUBES USING ITERATIVE  
ANALYTICAL APPROACH**

**EDWIN LIM CHUI SENG**

**UNIVERSITI TUNKU ABDUL RAHMAN**

**EVALUATION OF HIGH TEMPERATURE BOILER TUBES USING  
ITERATIVE ANALYTICAL APPROACH**

**EDWIN LIM CHUI SENG**

**A project report submitted in partial fulfilment of the  
requirements for the award of Bachelor of Engineering  
(Hons.) Mechanical Engineering**

**Faculty of Engineering and Science  
Universiti Tunku Abdul Rahman**

**April 2013**

## DECLARATION

I hereby declare that this project report is based on my original work except for citations and quotations which have been duly acknowledged. I also declare that it has not been previously and concurrently submitted for any other degree or award at UTAR or other institutions.

Signature : EDWIN LIM CHUI SENG

Name : EDWIN LIM CHUI SENG

ID No. : 09UEB05827

Date : 30 APRIL 2013

**APPROVAL FOR SUBMISSION**

I certify that this project report entitled **“EVALUATION OF HIGH TEMPERATURE BOILER TUBES USING ITERATIVE ANALYTICAL APPROACH”** was prepared by **EDWIN LIM CHUI SENG** has met the required standard for submission in partial fulfilment of the requirements for the award of Bachelor of Engineering (Hons.) Mechanical Engineering at Universiti Tunku Abdul Rahman.

Approved by,

Signature : \_\_\_\_\_

Supervisor : MR YEO WEI HONG

Date : 30 APRIL 2013

The copyright of this report belongs to the author under the terms of the copyright Act 1987 as qualified by Intellectual Property Policy of Universiti Tunku Abdul Rahman. Due acknowledgement shall always be made of the use of any material contained in, or derived from, this report.

© 2013, Edwin Lim Chui Seng. All right reserved.

*This page is specially dedicated to  
my beloved family and friends for their  
infinite guidance and encouragement*

## **ACKNOWLEDGEMENTS**

My deepest gratitude is dedicated specially to my project supervisor, Mr. Yeo Wei Hong of Universiti Tunku Abdul Rahman (UTAR) for his invaluable advice, guidance and enormous patience throughout the development of this project. I would also like to thank the engineers of Kuala Langat Power Plant Sdn. Bhd. (formerly known as Genting Sanyen Power Sdn. Bhd.) who had contributed their time and effort in providing me with all necessary information for this project, which indirectly making this project fruitful.

Last but not least, I would also like to express my utmost gratitude to my project partner, Mr. Ang Wei Bing for his helping hand and continuous motivation to materialise the objectives of this project.

## **EVALUATION OF HIGH TEMPERATURE BOILER TUBES USING ITERATIVE ANALYTICAL APPROACH**

### **ABSTRACT**

Heat recovery steam generator is used to harvest the exhaust flue gas expelled from gas turbine to generate steam for power generation in steam turbine-generator. The steam is generated via the application of boiler tubes. After several years of operation, excessive scale thickness and severe wall thinning on the tube can lead to tube rupture. Therefore, a reliable system based on the predictive maintenance philosophies is needed to monitor and give an early notice of tube failure. In this project, an iterative analytical program has been adopted to evaluate the behaviour and performance of boiler tubes in terms of tube temperature, heat flux, oxide-scale growth, creep strength, material hardness and hoop stress. A sample model acquired from a research paper was used to develop seven other tube models by varying several key parameters suited for this study. From the investigations conducted on the seven tube models, it was observed that higher steam pressure, thinner tube geometry and the existence of wall thinning effect could result in a higher hoop stress and shorter creep life. The tube life was also influenced by the tube metal average temperature. The contributing factors to the increase in tube average temperature due to high surface heat flux, increase in scale thickness and its growth rate and reduction in hardness. These contributing factors were caused by the change in input parameters such as thick tube geometry, low steam mass flow rate, high flue gas temperature and mass flow rate. On the other hand, a comparison between two tube grades; SA213-T12 and SA213-T22 showed that the later has a better creep strength, hardness and oxide-scale growth performance due to the presence of higher Chromium and Molybdenum compositions within the tube.

## TABLE OF CONTENTS

<b>DECLARATION</b>	<b>ii</b>
<b>APPROVAL FOR SUBMISSION</b>	<b>iii</b>
<b>ACKNOWLEDGEMENTS</b>	<b>vi</b>
<b>ABSTRACT</b>	<b>vii</b>
<b>TABLE OF CONTENTS</b>	<b>viii</b>
<b>LIST OF TABLES</b>	<b>xi</b>
<b>LIST OF FIGURES</b>	<b>xii</b>
<b>LIST OF SYMBOLS / ABBREVIATIONS</b>	<b>xv</b>
<b>LIST OF APPENDICES</b>	<b>xvii</b>

### CHAPTER

<b>1</b>	<b>INTRODUCTION</b>	<b>18</b>
	1.1 Background on Heat Recovery Steam Generator	18
	1.2 Problem Statement	19
	1.3 Aim and Objectives	19
	1.4 Scope of Research	20
	1.5 Outline of Thesis	20
<b>2</b>	<b>LITERATURE REVIEW</b>	<b>22</b>
	2.1 Industrial Steam Generators and Heat Recovery Boilers	22
	2.2 Common Boiler Tube Materials	24
	2.3 Common Failure Mechanisms in Boiler Tube	27
	2.3.1 Waterside Corrosion and Scale Deposition in Boiler Tubes	28

2.3.2	Fireside Erosion-Corrosion and Wall Thinning on Boiler Tubes	31
2.3.3	Tube Overheating and Creep Formation on Boiler Tubes	33
2.4	Simulation Approach in Analysing Failure Mechanism	35
2.5	Fundamental Theories Related to Evaluation of Boiler Tubes	37
2.5.1	Heat Transfer Mechanism	37
2.5.2	Stresses on the Boiler Tube	43
2.5.3	Larson-Miller Parameter	44
2.5.4	Boiler Tube Strength	45
2.6	Summary	46
<b>3</b>	<b>METHODOLOGY</b>	<b>48</b>
3.1	Iterative Analytical Method in MATLAB	48
3.2	Case A – Exponent Rate Comparison in Kinetic of Oxidation	52
3.3	Case B – Performance Analysis on Boiler Tubes	53
3.4	List of Cases and Models	53
3.5	Time Step Specification	56
<b>4</b>	<b>RESULTS AND DISCUSSIONS</b>	<b>57</b>
4.1	Case A – Exponent Rate Comparison in Kinetic of Oxidation	57
4.2	Case B – Performance Analysis on Boiler Tubes	62
4.2.1	Effect of Tube Thickness	62
4.2.2	Effect of Flue Gas Temperature	65
4.2.3	Effect of Steam Mass Flow Rate	66
4.2.4	Effect of Mass Flow Rate of Flue Gas	69
4.2.5	Effect of Steam Pressure	71
4.2.6	Effect of Wall Thinning	74
4.2.7	Effect of Tube Material with Different Cr and Mo Content	78

4.2.8	Summary of Case B	80
<b>5</b>	<b>CONCLUSIONS AND RECOMMENDATIONS</b>	<b>82</b>
5.1	Conclusions	82
5.2	Recommendations	83
	<b>REFERENCES</b>	<b>85</b>
	<b>APPENDICES</b>	<b>89</b>

## LIST OF TABLES

<b>TABLE</b>	<b>TITLE</b>	<b>PAGE</b>
2.1	Ferritic Alloys Used in Boiler Construction	25
2.2	Alloying Elements and Its Functions	25
2.3	Material Properties for SA213-T12 and SA213-T22	27
2.4	Value of Exponent Rate, n	30
3.1	List of Input Geometries and Its Respective MATLAB Variables	54
3.2	Constant Parameters for Case A	54
3.3	List of Models for Case A	55
3.4	Constant Parameters for Case B	55
3.5	List of Models for Case B	56
3.6	Time Step in Iterative Procedure	56
4.1	Percentage Error for Exponent Rate of $n = 0.5$	57
4.2	Percentage Error for Exponent Rate of $n = 0.33$	58
4.3	Some Output Results from MATLAB for Model 7 in Time Step. The Results is Used to Determine the LMP and CCDMG Values	77

## LIST OF FIGURES

FIGURE	TITLE	PAGE
2.1	Water Tubes Used in Natural Water Circulation HRSG (Spirax Sarco 2011. p. 240)	23
2.2	Three Stage/Pass of Hot Gas Path in PB (Spirax Sarco 2011. p. 231)	24
2.3	Scale Deposition in the Interior Wall of LPCSH-II (Ranjbar 2007. p. 622)	29
2.4	Photographs on Heavy Wall Thinning on the Superheater Tubes (Chandra, Kain and Dey 2010. p. 63)	32
2.5	Microstructure of Creep Fracture Mechanism (Jones 2004. p. 878)	34
2.6	Temperature Distribution of Water Tube Simulated in ANSYS (Purbolaksono et al., 2010. p. 103)	36
2.7	Model of Water Boiler Tube (Purbolaksono et al., 2010. p. 100)	38
2.8	Typical Arrangements of the Bare Tubes in a Boiler (a) Inline; (b) Staggered (Purbolaksono et al., 2010. p. 101)	41
2.9	Complete Thermal Circuit of the Model of Water Boiler Tube	42
3.1	Simple Flow Chart on the Analytical Procedure in MATLAB	49
4.1	Scale Thickness versus Service hour <sup>n</sup> for Model A	58
4.2	Scale Thickness versus Service hour <sup>n</sup> for Model B	59
4.3	Scale Thickness versus Service hour <sup>n</sup> for Model C	59

4.4	Scale Thickness versus Service hour <sup>n</sup> for Model D	60
4.5	Scale Thickness versus Service hour <sup>n</sup> for Model E	60
4.6	Scale Thickness versus Service hour <sup>n</sup> for Model F	61
4.7	Scale Thickness versus Service hour <sup>n</sup> for Model G	61
4.8	Hoop Stress versus Service Hour for Model 1 and Model 2 with Different Tube Thickness	62
4.9	Cumulative Creep Damage versus Service Hour for Model 1 and Model 2 with Different Tube Thickness	63
4.10	Stresses versus Service Hour Plot for Model 1 for 3.5 mm thickness	64
4.11	Stresses versus Service Hour Plot for Model 2 for 4.5 mm thickness	64
4.12	Tube Metal Average Temperature versus Service Hour for Model 1 and Model 3 with Different Flue Gas Temperature	65
4.13	Cumulative Creep Damage versus Service Hour for Model 1 and Model 3 with Different Flue Gas Temperature	66
4.14	Tube Metal Average Temperature versus Service Hour for Model 1 and Model 4 with Different Steam Mass Flow Rate	67
4.15	Scale Thickness versus Service Hour for Model 1 and Model 4 with Different Steam Mass Flow Rate	67
4.16	Hardness Vickers Plot for Model 1 and Model 4 with Different Steam Mass Flow Rate	68
4.17	Scale Thickness versus Service Hour for Model 1 and Model 5 with Different Flue Gas Mass Flow Rate	70
4.18	Kinetic of Oxidation Plot for Model 1 and Model 5 with Different Flue Gas Mass Flow Rate	70
4.19	Outer Tube Surface Heat Flux versus Service Hour for Model 1 and Model 5 with Different Flue Gas Mass Flow Rate	71

4.20	Hoop Stress versus Service Hour for Model 1 and Model 6 with Different Steam Pressure	72
4.21	Cumulative Creep Damage versus Service Hour for Model 1 and Model 6 with Different Steam Pressure	72
4.22	Stresses versus Service Hour for Model 6 with Steam Pressure of 8 MPa	73
4.23	Hoop Stress versus Service Hour for Wall Thinning Comparison between Model 1 and Model 7	74
4.24	Stresses versus Service Hour for Wall Thinning Effect in Model 7	75
4.25	Tube Metal Average Temperature for Wall Thinning Comparison between Model 1 and Model 7	76
4.26	Cumulative Creep Damage Plot for Wall Thinning Comparison between Model 1 and Model 7	77
4.27	Cumulative Creep Damage Plot for Tube Material Comparison between Model 1 and Model 8	79
4.28	Kinetic Oxidation Plot for Tube Material Comparison between Model 1 and Model 8	79
4.29	Hardness Plot for Tube Material Comparison between Model 1 and Model 8	80

## LIST OF SYMBOLS / ABBREVIATIONS

$d_i$	Inner diameter of tube, $m$
$d_o$	Outer diameter of tube, $m$
$h_g$	Convection coefficient of flue gas, $W/(m^2 \text{ } ^\circ C)$
$h_s$	Convection coefficient of steam, $W/(m^2 \text{ } ^\circ C)$
$k_m$	Thermal conductivity of tube metal, $W/(m \text{ } ^\circ C)$
$k_o$	Thermal conductivity of oxide-scale, $W/(m \text{ } ^\circ C)$
$l$	Tube length, $m$
$\dot{m}_s$	Mass flow rate of steam, $kg/h$
$p$	Stream pressure, $MPa$
$q$	Heat transfer rate, $W$
$r_i$	Inner radius of tube, $m$
$r_o$	Outer radius of tube, $m$
$C_p$	Specific heat, $J/(kg \text{ } ^\circ C)$
$G$	Gas mass velocity, $kg/(h \text{ } m^2)$
$HV$	Vickers Hardness, $HV$
$L$	Tube length, $m$
$Nu$	Nusselt Number
$N_w$	Number of tube wide
$Pr$	Prandtl Number
$Re$	Reynolds Number
$R_t$	Thermal resistance, $^\circ C/W$
$S_t$	Transverse pitch, $m$
$T_g$	Flue gas temperature, $^\circ C$
$T_s$	Steam temperature, $^\circ C$
$W_g$	Mass flow rate of flue gas, $kg/h$

$\mu_g$	Dynamic viscosity of flue gas, $(N\ s)/m^2$
$\mu_s$	Dynamic viscosity of steam, $(N\ s)/m^2$
$\sigma_h$	Hoop stress, $MPa$
ASM	American Society for Metals
ASME	American Society of Mechanical Engineers
ASTM	American Society for Testing and Materials
EPRI	Electric Power Research Institute
HRSG	Heat Recovery Steam Generator
HV	Hardness Vickers
KLPP	Kuala Langat Power Plant
LMP	Larson-Miller Parameter
PB	Packaged Boiler

**LIST OF APPENDICES**

<b>APPENDIX</b>	<b>TITLE</b>	<b>PAGE</b>
A	Larson-Miller Parameter chart for SA213-T12 (Smith 1973)	89
B	Larson-Miller Parameter chart for SA213-T22 (Smith 1971)	90
C	Output results recorded by MATLAB at specified time steps for Case B – Performance Analysis on Boiler Tubes	91
D	Sample Calculation on Minimum Tube Wall Thickness	101

## **CHAPTER 1**

### **INTRODUCTION**

#### **1.1 Background on Heat Recovery Steam Generator**

Heat Recovery Steam Generator (HRSG) is a large scale industrial boiler use to generate steam from water source. This principle is almost similar to our daily routine in boiling water in a kettle. In order to change water into steam, heat is added into the system by means of combustion of fossil fuels, electricity and even the Sun.

However, conversion process of water into steam in a large scale industrial boiler involves a large amount of operating cost. Due to cost concern, engineers have come out with a solution to increase efficiency of steam production with the same amount of fuel (Steingress 1970). It is done by increasing the heating surface area in contact with the water. This enables the heat to be fully utilised and not lost to surrounding. This is achieved by the application of boiler tubes. Boiler tubes are normally made of ferritic steels, combined with other alloying elements such as Nickel, Molybdenum, Chromium, Manganese and etcetera to improve its mechanical properties in order to withstand extreme operating pressure and temperature.

Boiler tubes can be categorised into water tube and fire tube. A water tube refers to the flow of water inside the tube with combustion gasses flow externally. On the other hand, a fire tube refers to combustion gasses that flow inside the tube with the tube being surrounded by water on its exterior. The analytical evaluation in this project will only consider for the water tube category.

## **1.2 Problem Statement**

HRSG obtain its heat source from exhaust (flue) gas expelled from gas turbine. High thermal exposure and inefficient heat transfer from the flue gas into the water contained in water tubes due to the development of scales on the internal tube wall results in creep formation. The boiler tubes condition worsen with wall thinning effect on the exterior tube wall as it promotes higher hoop stress on the tube and thus, shortens the life span of the tubes. With the existence and interaction between thick scales and wall thinning, the life span of the tubes could further reduced.

As the life of the boiler tube reaches its limit, failure such as rupture will occur. Since HRSG is operated at elevated temperature and pressure, any tube rupture will definitely cause major physical damages to the nearby tubes and the boiler's water wall. These lead to a higher repair cost. In some extreme cases, it may also threaten humans' life due to the high pressure 'explosion'. Therefore, it is important to carry out a proper study in order to mitigate such problems.

## **1.3 Aim and Objectives**

The aim of this research is to evaluate the performance of boiler tubes using a developed MATLAB code which is based on one-dimensional heat transfer model.

Several objectives have been identified in this research and are stated as follow:

1. To perform iterative analytical study on boiler tubes by applying the developed MATLAB codes.
2. To evaluate on the effect of varying several key parameters towards the behaviour of boiler tubes.
3. To investigate and compare the performance between two boiler tube grades.

## **1.4 Scope of Research**

A research has been conducted to study the behaviour of the boiler tubes under different loading parameters by implementing the developed iterative analytical procedure in MATLAB. This iterative program was based on a simple one-dimensional heat transfer model.

Various different parameters have been selected for this study which includes tube geometry, flue gas temperature, steam mass flow rate, flue gas mass flow rate, steam pressure and wall thinning effect. Any behavioural changes in term of hoop stress, tube metal average temperature, surface heat flux, tube hardness, creep damage, scale thickness and its growth rate have been analysed, discussed and presented in this project.

From the outcome and understanding in this project, an investigation was then carried out to compare the performance between two tube grades; SA213-T12 and SA213-T22 in terms of creep strength, tube hardness and corrosion resistance. The difference between these tubes is that SA213-T22 tube grade has higher Chromium and Molybdenum content as compared to SA213-T12.

## **1.5 Outline of Thesis**

The layout in this report is organised based on the outline described below:-

Chapter 2 – Literature Review describes the types of Heat Recovery Steam Generators and Heat Recovery Boilers and their usages. The general boiler tube materials/grades and its properties are briefly explained. The common boiler tube failure mechanisms and several research/theoretical findings that are of the interest in this project have been highlighted.

Chapter 3 – Methodology explains about the steps in the iterative analytical method that is used for evaluation purpose in this project. The details on the cases

and models are highlighted. The input geometries and all necessary parameters for the MATLAB simulation are tabulated accordingly in this chapter.

Chapter 4 – Results and Discussion displays the graphical representation of the output data recorded by MATLAB. Discussions and comments are given based on the plot interpretation and comparison between models. A simple summary is concluded for each study.

Chapter 5 – Conclusions and Recommendations highlights on the overall summary of this project. Some recommendations on future works are suggested.

## **CHAPTER 2**

### **LITERATURE REVIEW**

#### **2.1 Industrial Steam Generators and Heat Recovery Boilers**

As mentioned in the previous chapter, both steam generators and heat recovery boilers are used to convert water from saturated liquid phase into steam at a specific pressure through heat addition. By varying the operating pressure and the amount of heat added, different types of steam will be produced such as low pressure steam and high pressure superheated steam. The main source of heat is obtained through the burning of fossil fuels such as natural gases, coals and petroleum. Steam is used in nearly every industry to facilitate their processes and it is well known that steam generators and heat recovery boilers are important to both power and process plants (Ganapathy 2003). High pressure superheated steam is utilised by power generation industries to drive their steam turbines while low pressure saturated steam is used by various industries for industrial processes such as heating and drying. Generally, there are two types of boilers which are the vertical tube HRSG and horizontal tube Package Steam Generators or also known as Packaged Boiler (PB). The vertical and horizontal tubes indicate the arrangement of the boiler tubes in the boiler.

HRSG is a type of heat exchanger that recovers waste heat from hot (flue) gas stream. The heat recovered turn water inside the water tube to produce steam which is used to drive a steam turbine-generator in a combined cycle power plant or to be used for other application in various industries. Flue gas from gas turbine exhausting into a HRSG in a combined cycle power plant is the most efficient electric generating system known today (Ganapathy 2003). HRSG has the advantage of

higher steam production rate and high level of operating safety. The common type of HRSG is the natural water circulation type where the water circulates by virtue of density difference between the water in the downcomer and upriser. Figure 2.1 shows the natural water circulation in a HRSG.

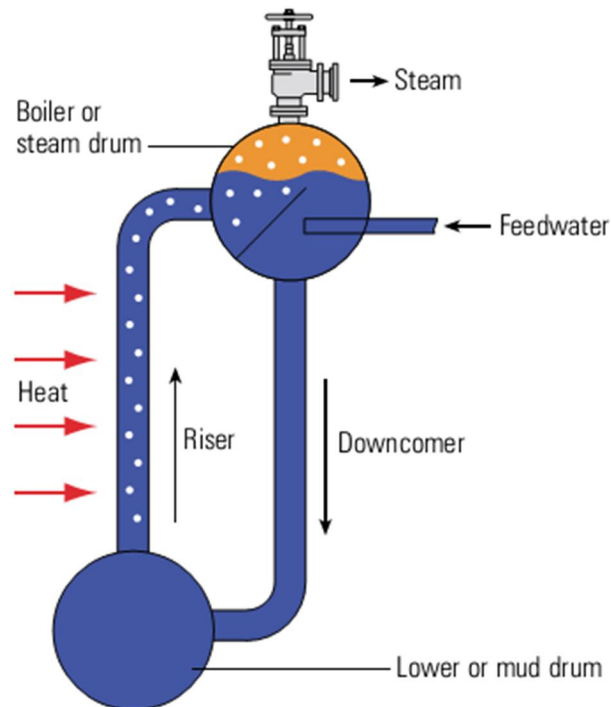


**Figure 2.1: Water Tubes Used in Natural Water Circulation HRSG (Spirax Sarco 2011. p. 240)**

On the other hand, PB is a type of fire tube boiler where the combustion hot air from the furnace is passed through one or more tubes running through a sealed container of water called the steam drum. Figure 2.2 shows the construction of an industrial PB. The number of pass or stages in the PB depends on the amount of gas flow. With small amount of gas flows, one may consider multi pass design of PB, which can reduce the overall length of the boiler tubes (Ganapathy 2003). The heat is transferred from hot gas to the water by thermal conduction where it boils the water and generates steam. PB is unable to generate a high pressure superheated steam and has a low steam production rate. However, PB has the advantage of higher steam storage capacity compared to HRSG.

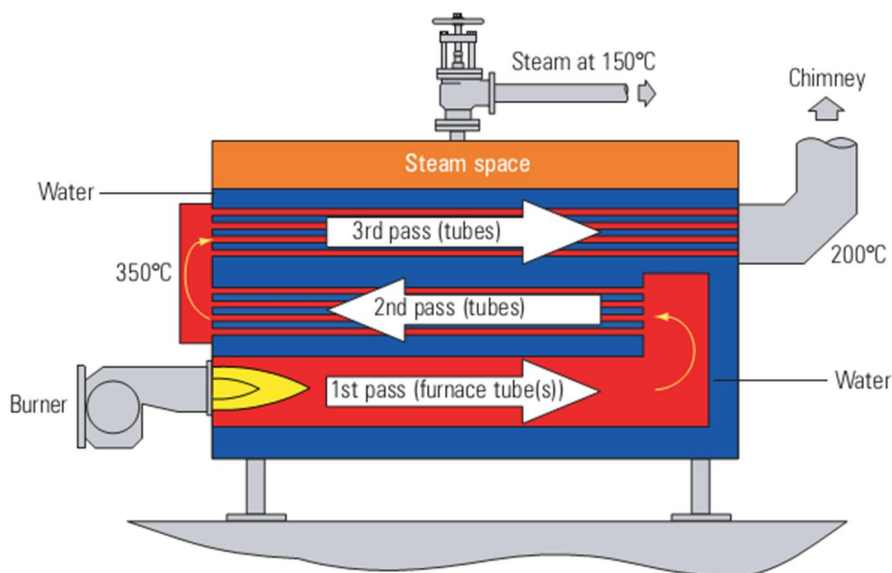


**Figure 2.2: Three Stage/Pass of Hot Gas Path in PB (Spirax Sarco 2011. p. 231)**

## 2.2 Common Boiler Tube Materials

Boiler tubes are usually manufactured using alloy materials which can withstand both high temperature from the flue gases and high pressure steam generation within the tube. The use of high temperature heat resistant alloys not only improves the supercritical steam quality for better HRSG efficiency, they also allow reduction in volumes of material for fabrication, both which promotes positive economy benefits.

According to Viswanathan (1993), boiler tubes are often categorised into three groups of alloys; carbon steels, ferritic alloys and austenitic stainless alloys in which all the tubes are then graded according to its material compositions. The material grades listed by the author are based on the American Society of Mechanical Engineers (ASME) standards. Some of the alloy grades that are commonly used as superheater and reheater tubes are listed in the Table 2.1.

**Table 2.1: Ferritic Alloys Used in Boiler Construction**

Nominal Compositions of Ferritic Alloys	ASME Specs.	Grade*	Composition (%)				
			P	S	Si	Cr	Mo
5Cr-0.5Mo	SA213	T5	0.030	0.030	0.50	4.0-6.0	0.45-0.65
9Cr-1Mo		T9	0.030	0.030	0.25-1.0	8.0-10.0	0.90-1.10
1.25Cr-0.5Mo		T11	0.030	0.030	0.50-1.0	1.0-1.50	0.44-0.65
1Cr-0.5Mo		T12	0.045	0.045	0.50	0.8-1.25	0.44-0.65
2.25Cr-1Mo		T22	0.030	0.030	0.50	1.9-2.60	0.87-1.13

\*All tube grades have same compositions of Carbon at 0.15% and Manganese at 0.3-0.6%  
(Viswanathan 1993. p. 186)

From Table 2.1, it is observed that different material grades consist of different percentage of compositions of alloying elements. These alloying elements are desirable as it helps to improve the mechanical properties of the tube. Table 2.2 shows the function of each alloying elements.

**Table 2.2: Alloying Elements and Its Functions**

Alloying Element	Functions
Carbon (C)	<ul style="list-style-type: none"> <li>• Increase solid-solution strength, hardness and hardenability</li> </ul>
Manganese (Mn)	<ul style="list-style-type: none"> <li>• Improve solid solution strength, hardness and hardenability</li> <li>• Counteracts brittleness caused by sulfur</li> <li>• Improve wear and abrasion resistance</li> </ul>
Chromium (Cr)	<ul style="list-style-type: none"> <li>• Increase solid-solution strength, hardness and hardenability</li> <li>• Increase resistance to corrosion and high temperature oxidation</li> <li>• Improve wear and abrasion resistance</li> <li>• Provide high temperature strength</li> </ul>
Molybdenum (Mo)	<ul style="list-style-type: none"> <li>• Increase solid-solution strength, hardness and hardenability</li> <li>• Improves high temperature properties such as creep strength</li> <li>• Counteracts temper embrittlement</li> <li>• Enhance corrosion resistance in stainless steel</li> </ul>
Sulfur (S)	<ul style="list-style-type: none"> <li>• Considered as impurity in most steels</li> <li>• Improve machinability</li> </ul>

**Table 2.2: (Continued)**

Alloying Element	Functions
Silicon (Si)	<ul style="list-style-type: none"> <li>• Increase solid-solution strength, hardness and hardenability</li> <li>• Remove oxygen in molten steel</li> <li>• Improves oxidation resistance, electrical and magnetic properties</li> <li>• Promotes decarburisation</li> </ul>
Phosphorus (P)	<ul style="list-style-type: none"> <li>• Considered as impurity in most steels</li> <li>• Increase strength and hardness in in low-carbon steels</li> <li>• Improve machinability and promotes temper embrittlement</li> </ul>

(ASM International 2002. p. 3)

The material grade selection may vary depending on the location where the tube will be installed and the operation requirements of the boiler. Among these factors, the most prominent feature to be deeply considered is the tube strength and the corrosion resistance properties at high temperature and pressure. From the list in Table 2.1, only two grades; SA213-T12 and SA213-T22 have been considered in this project because they are widely used by major power plants in Malaysia.

Table 2.3 shows the material properties for high temperature application for both alloy grade SA213-T12 and SA213-T22 obtained from ASME (2004b, p. 30). From the table, it is observed that alloy T22 (short notation for SA213-T22) has higher allowable stress value than T12 (short notation for SA213-T12). This shows that T22 can withstand at a much higher stress level before the tube is in critical state prior to failure. The values from Table 2.3 are used as one of the evaluation criteria to ensure the integrity of the tube.

**Table 2.3: Material Properties for SA213-T12 and SA213-T22**

Alloy		SA-213-T12	SA-213-T22
Min. Tensile Strength (MPa)		415	415
Min. Yield Strength (MPa)		220	205
Maximum Allowable Stress (MPa) at respective Average Metal Temperature	65°C	117	118
	100°C	116	118
	125°C	114	116
	150°C	114	114
	200°C	114	114
	250°C	114	114
	300°C	113	114
	325°C	112	114
	350°C	110	114
	375°C	109	114
	400°C	107	114
	425°C	106	114
	450°C	103	114
	475°C	101	100
	500°C	88.3	80.9
	525°C	61.9	64
	550°C	40.3	47.7
575°C	26.4	34.5	
600°C	17.3	23.5	
625°C	11.7	15.5	
650°C	7.4	9.39	

(ASME 2004b. p. 30)

### 2.3 Common Failure Mechanisms in Boiler Tube

In order to meet the growing demand of energy, HRSG are often required to operate at high temperatures and pressures to increase the heating efficiency. As a consequence, the boiler tubes often experience frequent event of failures. These failure mechanisms are very much similar to the mechanism that have been reported by Robert and Harvey (1991) and EPRI (2007). The primary factors influencing the repetition of tube failures include:-

- a) Wrong decision in the corrective and preventive actions
- b) Lack of information in previous tube failures' reports
- c) The standard operating and maintenance procedures are not carried out properly by the plant engineers and operators

The failure mechanisms and the specific analysis approach that are related to this project will be discussed further in the following subsections.

### **2.3.1 Waterside Corrosion and Scale Deposition in Boiler Tubes**

Waterside corrosion is often present in any water tube boilers. This type of corrosion greatly influences the reliability of the heat recovery boilers as it deteriorates the tube material. The deposition of scale due to waterside corrosion is caused by the chemical reaction between the tube material and the chemical composition inside the water. These corrosion failures are the result of ineffective control of water chemistry. According to the guidelines provided by EPRI (2007), corrosion also depends on the number of operating cycles because most of the upsets in water chemistry occur during the start-up prior to steady-state operation.

The intensity of corrosion greatly depends on the pH level of the water. The rate of corrosion increases at high temperature due to the increase in water acidity. Therefore, the water used in industrial boilers is dosed with certain amount of caustic to maintain its alkalinity. However, overdosing caustic can also lead to caustic corrosion. The build-up of boiler water impurities causes two kinds of accelerated on-load corruptions (Natarajan and Kumaresh 2006). The first kind is caused by caustic attack from the boiler water treatment additives while the second kind is caused by chloride impurities which are acidic or will become acidic when heated up with the elevating boiler temperature. In addition, the water used for steam production may contain gaseous impurities and dissolve solids which may result in scaling in the boiler tube. Khajavi et al. (2007) added on to the findings of caustic

corrosion. Based on their research, caustic corrosion is caused by the presence of sodium hydroxide (NaOH) that reacts with the metal wall to produce depressions. The tendency for a metal to react with NaOH is based on the amphoteric nature of the iron oxides and the concentration of NaOH. Since the primary function of caustic is to maintain the alkalinity of water to avoid acid corrosion, too concentrated of caustic can also leads to corrosion. Besides caustic corrosion, the authors had also identified phosphate corrosion as one of the contributing corrosion on industrial boilers. Phosphate corrosion exists due to the reaction of sodium phosphate with the tube material which produces a by-product of iron phosphate.

Failure analysis carried out by Ranjbar (2007) indicated that the most prevailing corrosion mechanism occurred in reheater tubes were caustic corrosion. Figure 2.3 shows the scales that were formed inside Low Pressure Convective Superheater, second stage (LPCSH-II).



**Figure 2.3: Scale Deposition in the Interior Wall of LPCSH-II (Ranjbar 2007. p. 622)**

Apart from the effect of corrosion, the oxide-scale growth can also be expressed as a function of tube temperature and time of exposure (Viswanathan 1993). For instance, tube temperature increases during its lifetime due to the oxide build up in the interior of the tube which insulates the tube from the flow of water.

As the tube temperature increase, the scale deposition rate increases and this phenomenon repeat as a cycle which obeys a specific rate law. Table 2.4 shows various exponent rates,  $n$  proposed by several researchers to estimate the oxide-scale growth kinetics. An approximate expression for Cr-Mo steels by these groups of researchers is presented in Equation 2.1.

**Table 2.4: Value of Exponent Rate,  $n$**

Exponent rate, $n$	Proposed by
$\frac{1}{3.0}$	Rehn and Apblett (1981)
$\frac{1}{2.0}$	Dewitte and Stubbe (1986)
$\frac{1}{2.1}$ to $\frac{1}{2.6}$	Paterson and Rettig (1987)
$\frac{1}{2.6}$ to $\frac{1}{3.0}$	Paterson (1992)

(Viswanathan, Sarver and Tanzosh 2006. p. 257)

$$x = kt^n \quad (2.1)$$

where

$x$  = oxide-scale thickness, mm

$k$  = oxide-scale growth rate constant

$t$  = exposure time, h

$n$  = exponent rate

Since both the exponent value of  $\frac{1}{3.0}$  and  $\frac{1}{2.0}$  proposed by Rehn and Apblett (1981) and Dewitte and Stubbe (1986) respectively are used for ferritic tubing, it is adopted in this project as both T12 and T22 grade tubes are made of ferritic alloys. Both of the  $n$  values are tested and compared in order to determine on which exponent rate is the most suitable for this project.

### 2.3.2 Fireside Erosion-Corrosion and Wall Thinning on Boiler Tubes

In power generation industries, wall thinning on the boiler tubes which lead to tube rupture is considered as one of the most feared effect that may possibly lead to major breakdown in their HRSGs. Besides affecting the production operations, a huge amount of cost is incurred to replace the damaged tubes.

The wall thinning effect is caused by excessive fireside tube erosion and corrosion on the outer surfaces of the tube. Since boiler tubes are exposed to an extremely high operating temperature and fast moving hot gas flow, any substances that are present in the flue gas that came into contact with the tube wall surface may chip off the tube material. This condition worsens if those substances have the right chemical compositions in causing corrosion to the tube.

There is no doubt that today; the price of a regular fuel oil is increasing. This motivates power generation and process industries to opt for heavy fuel oil as a cheaper fuel alternative to power up their gas turbines and boilers. However, the combustion of heavy fuel oil can produce corrosive particles that contain significant amount of vanadium, sulphur and chlorine. According to Hernas et al. (2004), the mixture of these contents could lead to an aggressive corrosion atmosphere and thus, accelerates the rate of corrosion. Besides, the corrosion rate is also amplified by the fluctuation in flue gas flow. With large combustion residue accumulated, it may further promote erosion and corrosion to the fireside wall of the boiler tubes (Awassada et al., 2010).

Boiler tube samples collected for failure analysis carried out by Chandra, Kain and Dey (2010) on superheater tubes with carbon steel grade of SA213-T22 (2.25Cr-1Mo) are shown in Figure 2.4. In their research, the formation of thick calcium sulphate deposited on the fireside tube wall and its spallation were the main cause of tube failure. Bare material exposed due to the spallation of calcium sulphate deposits caused formation of new thick oxide layer (corrosion) which accelerated the failure rate. Fry et al. (2011) agreed with the finding and stated that the erosion and corrosion mechanism was often found in the superheater and economizer region inside the boiler.

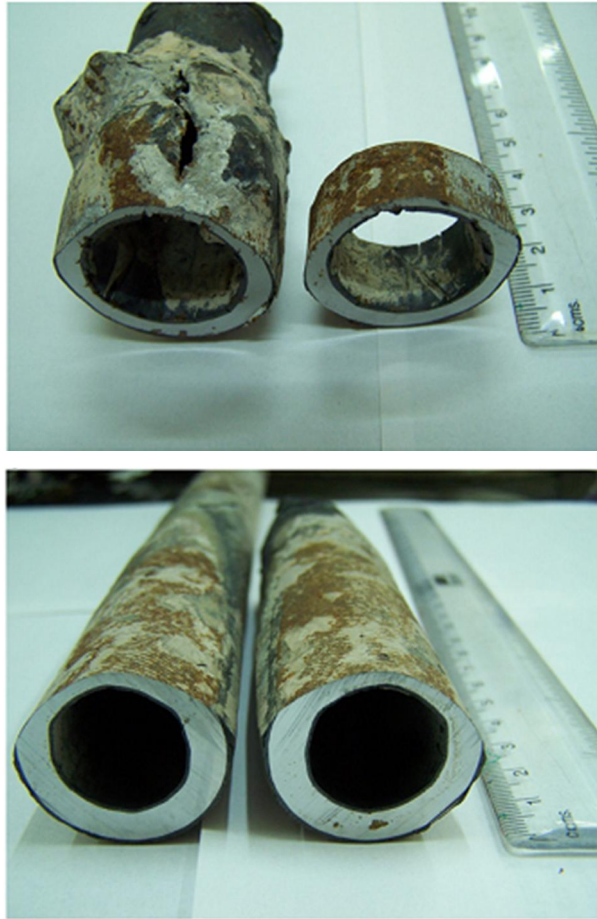


**Figure 2.4: Photographs on Heavy Wall Thinning on the Superheater Tubes (Chandra, Kain and Dey 2010. p. 63)**

Moles and Westwood (1982) had derived an equation for wall thinning in a superheater and reheater tubes. They assumed a linear corrosion rate and linear damage rule which is based on a conservative equation for creep damage. The wall thinning rate is defined in Equation 2.2.

$$K' = \frac{w_i - w_f}{w_i t_{op}} \quad (2.2)$$

where

$K'$  = wall thinning rate,  $h^{-1}$

$w_i$  = initial tube wall thickness, mm

$w_f$  = final tube wall thickness, mm

$t_{op}$  = operating time in service, h

However, this method is not use for the wall thinning analysis in this project. An alternative method is adopted to determine the wall thinning rate and the effect of wall thinning is performed through an iterative procedure. A more comprehensive discussion on this topic will be deliberated further in the next chapter.

Any boiler tubes operating below the minimum design tube thickness are considered to be in its critical state and are prone to failure. ASME (2004a, p. 15) has specified a formula to determine the minimum required thickness of tube. The formula is given as shown in Equation 2.3. It is to be noted that Equation 2.3 is based on the United States (US) customary units.

$$t = \frac{PD}{2S+P} + 0.005D + e \quad (2.3)$$

where

$t$  = minimum required tube thickness, in (1 in = 0.0254 m)

$P$  = design pressure, psi (1 psi = 0.006895 MPa)

$D$  = outer diameter of tube, in

$S$  = maximum allowable stress (based on average tube metal temperature), psi

$e$  = thickness factor (0.04 for expanded tubes; 0 for strength welded tubes)

### 2.3.3 Tube Overheating and Creep Formation on Boiler Tubes

Materials are prone to deformation under constant stress (load) at high temperature. The time-dependant and thermally assisted deformation of a component under stress is known as creep (Viswanathan 1993). If there is no further action taken to slow down the creep propagation, it will finally turn into rupture. This is one of the major problems faced by most of the power generation industries with their boiler tubes.

Based on the guidelines provided by EPRI (2007), creep formation on the boiler tubes are closely related tube overheating; either a long-term overheating or short-term overheating. Long-term overheating is describe as gradual increase in the

tube metal temperature and stress level above the design temperature over a long period of time which leads to metal yielding. On the other hand, short-term overheating refers to increase in tube metal temperature over a short period of time. Jones (2004) describes that anything that interferes with the cooling effect from the water flowing in the tube results in overheating. These interferences are identified to be oxide-scale from waterside corrosion and delamination in the tube wall which will provide an effective thermal barrier. Besides, the author states that ‘steam blanketing’ could also lead to creep-rupture. Steam blanketing is a layer of steam that separates the cooling water from the tube wall. This layer acts as an insulation to the tube from the circulating water where in the long term, it can cause tube overheating problems.

An investigation was carried out by Lee et al. (2009) on a superheater tube in coal power plant. From the investigation, it was observed that when the tube was heated more than the design temperature, formation of voids can be observed in the boundary between magnetite and spinel layer. After a long time, the void contents increased, causing adhesion weakness on the boundary layers which led to exfoliation of scales. In the end, creep-rupture occurred due to blockage of steam flow and the softening of tube structure induced by carbide coarsening at high metal temperature.

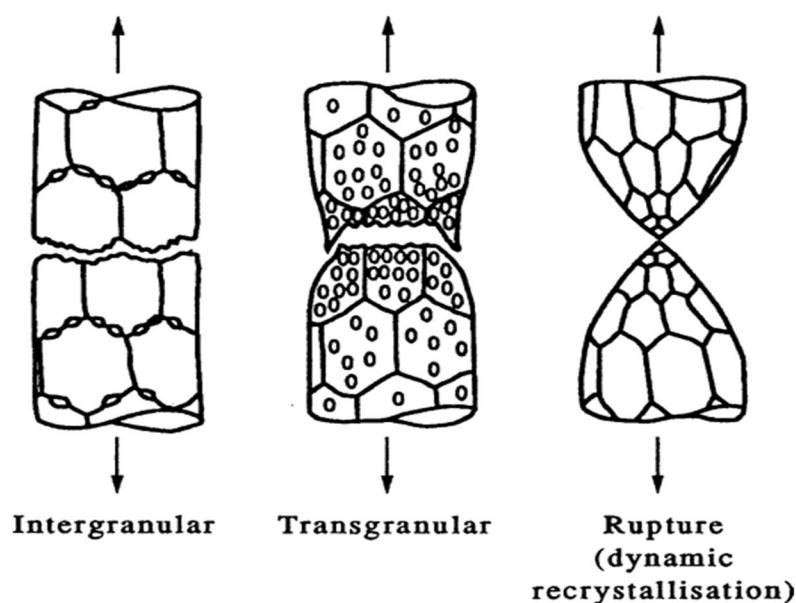


**Figure 2.5: Microstructure of Creep Fracture Mechanism (Jones 2004. p. 878)**

The evaluation of creep life in this project is carried out by applying the linear damage rule. Robinson (1938) had proposed a linear damage summation concept for predicting creep life under varying temperature. The time dependant creep life is expressed as shown in Equation 2.4.

$$\sum \frac{t_{service}}{t_{rupture}} = 1 \quad (2.4)$$

where

$t_{service}$  = service time at given stress and temperature, h

$t_{rupture}$  = rupture time at that stress and temperature, h

When Equation 2.4 reaches unity, the tube is said to have reached its creep life and tube failure is expected to occur.

## 2.4 Simulation Approach in Analysing Failure Mechanism

Simulation approaches are becoming famous these days as researchers are now aware of the importance of predictive maintenance. The issues of remaining life prediction have attracted considerable attention in the power generation industries (Mukhopadhyay, Dutta and Kushwaha 2001). Most of the researchers had come out with their own simulation models to study the failure mechanism of the boiler tube. The simulation results obtained are frequently compared with the actual field data and the results must be known of whether it had meet an agreement or otherwise. If the agreement is achieved, the simulation model can be useful to the related industries to predict the life of the boiler tubes.

For instance, Mukhopadhyay et al. (1999) had developed a finite element based fatigue monitoring system to monitor various components degradation in the power plant by converting the plant transients to temperature/stress responses using the Finite Element Method (FEM) and the transfer function approach. The author and his team had successfully implemented the system into use since the mid of 1996.

They furthered their study on the implementation of a dedicated software for online monitoring of creep, fatigue and creep-fatigue interaction (Mukhopadhyay, Dutta and Kushwaha 2001). Majidian and Saidi (2007) came out with the idea to predict the life of boiler tubes by using Fuzzy logic and Neural Network. Rahmani et al. (2009) made an attempt to use multipurpose best estimate thermal-hydraulic system code, RELAP5/Mod3.2 to simulate the steady state and transient dynamic behaviour of two-phase natural circulation steam boiler. Purbolaksono et al. (2010) came out with a technique in estimating the growth of oxide-scale in superheater and reheater tube using empirical formulae and finite element modelling in ANSYS. It was found that the scale thickness increases as temperature and time increases. They later implemented this technique as one of the condition monitoring for the water tube boilers. In their research, they had incorporated the oxide-scale growth in the boiler tubes into their simulation. The results obtained from the simulation were found to be of the same agreement to the actual data from power plant. The author and his team proceed further in their next research to estimate the heat flux and temperature in superheater and reheater tube by using the same mode of analysis. The ANSYS modelling is shown in Figure 2.6.

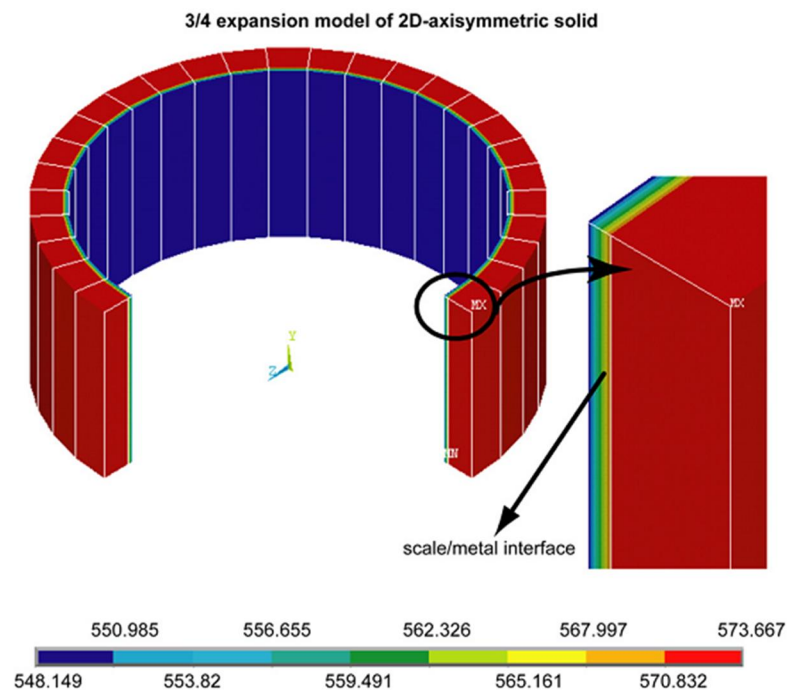


**Figure 2.6: Temperature Distribution of Water Tube Simulated in ANSYS (Purbolaksono et al., 2010. p. 103)**

## **2.5 Fundamental Theories Related to Evaluation of Boiler Tubes**

Extensive studies done by researchers in analysing the characteristics of boiler tubes are closely related with various well-established theories. In this project, the evaluation on the performance and behaviour of boiler tubes are carried out based on several related fundamental concepts. These concepts will be elaborated further in the next subsections.

### **2.5.1 Heat Transfer Mechanism**

Heat transfer is defined as the thermal energy in transit due to a spatial temperature difference (Incropera et al., 2007). Heat transfer processes can be grouped into three types of modes; conduction, convection and radiation. Conduction process starts when a temperature gradient is present in a stationary medium where the heat transfer is across that medium. Heat transfer between a surface and a moving contact fluid of different temperature is referred to as the convection process. On the other hand, radiation is the heat transfer between two non-contact surfaces at different temperatures by emitting energy in the form of electromagnetic waves.

In this research, only conduction and convection modes are taken into account. Based on the cross sectional model developed by Purbolaksono et al. (2010) in Figure 2.7, it is found that the steam section and the flue gas section experiences internal forced convection with turbulent flow and external forced convection due to cross flow respectively. The oxide and metal tube section experiences one-dimensional steady-state conduction.

In order to solve for the heat transfer rate,  $q$ ; Incropera et al. (2007) introduces a simple concept to estimate the temperature distribution over a period of time which is the thermal resistance circuit. This circuit may also be used to solve more complex systems such as composite wall structure as shown in Figure 2.7.

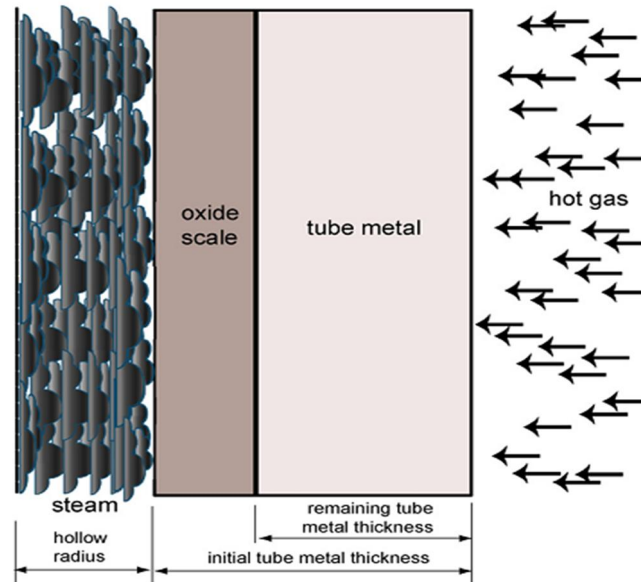


**Figure 2.7: Model of Water Boiler Tube (Purbolaksono et al., 2010. p. 100)**

The heat transfer equation and thermal resistance for both conduction and convection for circular hollow cylinder are given in Equation 2.5 to Equation 2.7.

$$q = \frac{T_{\infty,1} - T_{\infty,2}}{\sum R_{t,cond} + \sum R_{t,conv}} \quad (2.5)$$

$$R_{t,cond} = \frac{\ln\left(\frac{r_o}{r_i}\right)}{2\pi Lk} \quad (2.6)$$

$$R_{t,conv} = \frac{1}{2\pi r L h} \quad (2.7)$$

where

$q$  = rate of heat transfer, W

$T_{\infty,1} - T_{\infty,2}$  = overall temperature difference in the system, °C

$R_{t,cond}$  = thermal resistance for conduction, °C/W

$R_{t,conv}$  = thermal resistance for convection, °C/W

$L$  = tube length, m

$k$  = thermal conductivity of matter, W/(m °C)

$h$  = convection coefficient of fluid, W/(m<sup>2</sup> °C)

$r_o$  = outer radius, m

$r_i$  = inner radius, m

Convection coefficient of the steam,  $h_s$  and its correlation for fully developed turbulent flow in circular tubes can be expressed as shown in Equation 2.8 and Equation 2.9 and must operate at a specific range of conditions stated in Equation 2.10 (Incropera et al., 2007). The Reynolds Number and Prandtl Number in those expressions are expressed in Equation 2.11 and Equation 2.12.

$$h_s = Nu \times \frac{k_s}{d_i} \quad (2.8)$$

$$Nu = 0.023(Re_s)^{0.8}(Pr_s)^{0.4} \quad (2.9)$$

$$\text{Range of conditions;} \quad \left\{ \begin{array}{l} 0.7 \leq Pr \leq 160 \\ Re_s \geq 10000 \\ \frac{\text{tube length}}{\text{tube inner diameter}} \geq 10 \end{array} \right. \quad (2.10)$$

$$Re_s = \frac{\dot{m}_s}{900\pi d_i \mu_s} \quad (2.11)$$

$$Pr_s = \frac{\mu_s C p_s}{k_s} \quad (2.12)$$

where

$h_s$  = convection coefficient of steam, W/(m<sup>2</sup> °C)

$k_s$  = thermal conductivity of steam, W/(m °C)

$d_i$  = inner diameter of tube, m

$Nu$  = Nusselt Number

$Re_s$  = Reynolds Number for steam flow

$Pr_s$  = Prandtl Number for steam flow

$\dot{m}_s$  = mass flow rate of steam, kg/h

$\mu_s$  = dynamic viscosity of steam, (N s)/m<sup>2</sup>

$C p_s$  = specific heat of steam, J/(kg °C)

The values for  $\mu_s$ ,  $Cp_s$  and  $k_s$  can be obtained through simple two-dimension interpolation from tables given in Ganapathy (2003).

On the other hand, the conservative estimates for convection coefficient of the flue gas,  $h_g$  for forced convection of the flue gas over the bare tubes is given in Equation 2.13 and Equation 2.14 (Ganapathy 2003). The Reynolds Number and Prandtl Number in those equations can be determined from Equation 2.15 and Equation 2.17.

$$h_g = Nu \times \frac{k_g}{d_o} \quad (2.13)$$

$$Nu = 0.33(Re_g)^{0.6}(Pr_g)^{0.33} \quad (2.14)$$

$$Re_g = \frac{Gd_o}{3600\mu_g} \quad (2.15)$$

$$G = \frac{W_g}{N_w L(S_t - d_o)} \quad (2.16)$$

$$Pr_g = \frac{\mu_g Cp_g}{k_g} \quad (2.17)$$

where

$h_g$  = convection coefficient of flue gas, W/(m<sup>2</sup> °C)

$k_g$  = thermal conductivity of gas, W/(m °C)

$d_o$  = outer diameter of tube, m

$Nu$  = Nusselt Number

$Re_g$  = Reynolds Number for flue gas flow

$Pr_g$  = Prandtl Number for flue gas flow

$G$  = gas mass velocity, kg/(h m<sup>2</sup>)

$\mu_g$  = dynamic viscosity of flue gas, (N s)/m<sup>2</sup>

$W_g$  = mass flow rate of flue gas, kg/h

$N_w$  = number of tube wide/number of rows of tubes

$L$  = length of tube, m  
 $S_t$  = transverse pitch, m  
 $Cp_g$  = specific heat of flue gas, J/(kg °C)

The value of  $N_w$  and  $S_t$  are obtained based on tube arrangements shown in Figure 2.8. Note that Equation 2.16 is only applicable for inline tube arrangement.

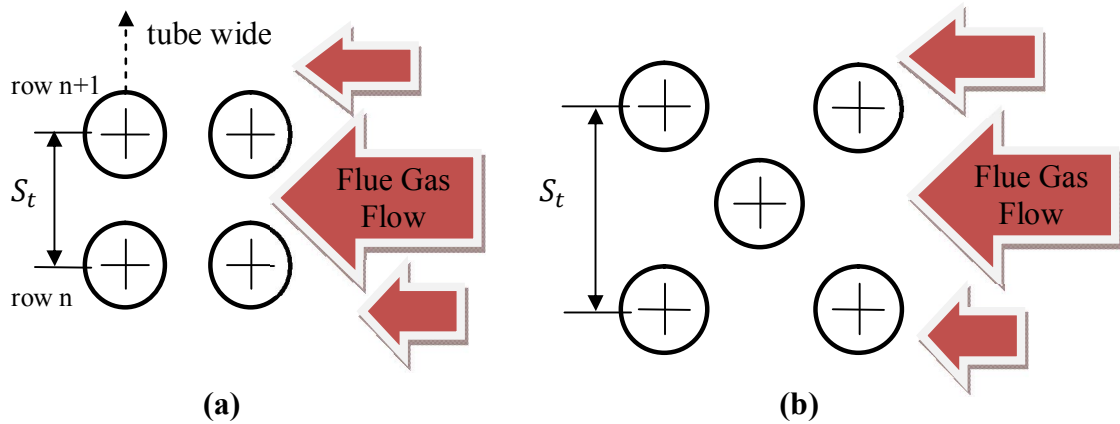


**Figure 2.8: Typical Arrangements of the Bare Tubes in a Boiler (a) Inline; (b) Staggered (Purbolaksono et al., 2010. p. 101)**

The gas properties, for instance,  $\mu_g$ ,  $Cp_g$  and  $k_g$  for gas mixtures are determined through the gas mixture equation as shown in Equation 2.18 to Equation 2.20 (Ganapathy 1994).

$$\mu_{mixture} = \frac{\sum y_i \mu_i \sqrt{MW_i}}{\sum y_i \sqrt{MW_i}} \quad (2.18)$$

$$Cp_{mixture} = \frac{\sum Cp_i MW_i y_i}{\sum MW_i y_i} \quad (2.19)$$

$$k_{mixture} = \frac{\sum y_i k_i^3 \sqrt{MW_i}}{\sum y_i \sqrt{MW_i}} \quad (2.20)$$

where

$i$  = gas constituent

$MW$  = molecular weight

$y$  = volume fraction

The values for  $\mu_i$ ,  $Cp_i$  and  $k_i$  for each individual gas compositions in flue gas can be obtained through simple one-dimension interpolation from a table provided in Ganapathy (2003).

The complete thermal circuit can be constructed based on the model in Figure 2.7 and is shown in Figure 2.9.

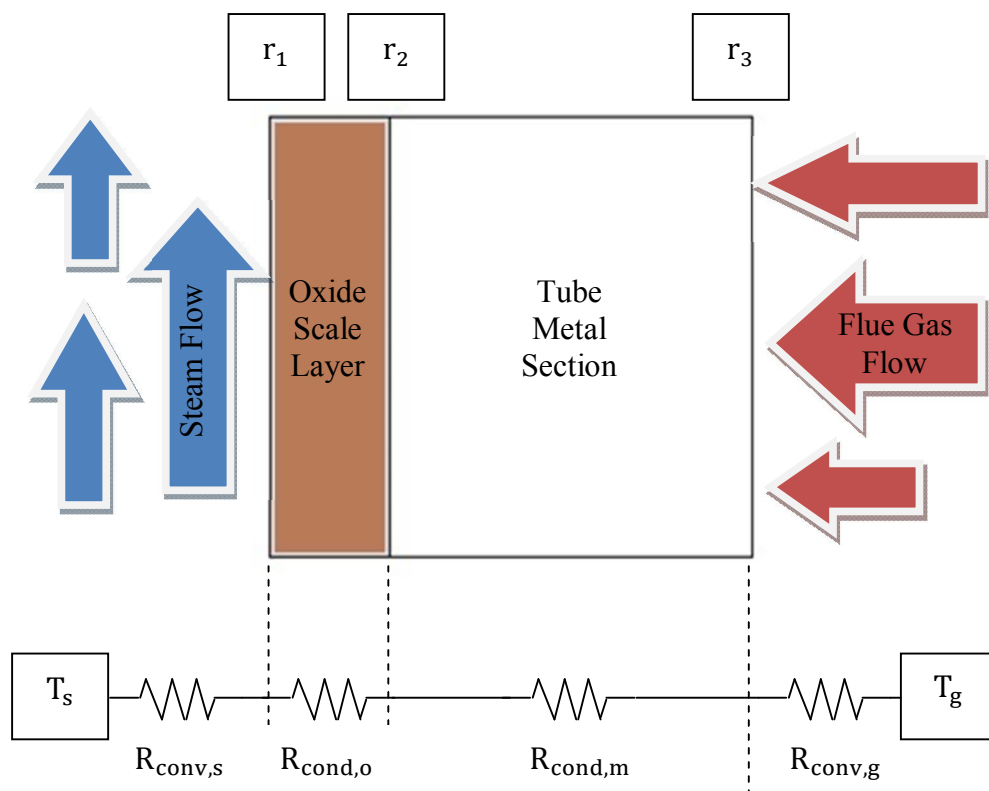


**Figure 2.9: Complete Thermal Circuit of the Model of Water Boiler Tube**

Therefore, the rate of heat transfer,  $q$  based on the thermal circuit model is expressed in Equation 2.21.

$$q = \frac{T_g - T_s}{\frac{1}{2\pi r_1 L h_s} + \frac{\ln\left(\frac{r_2}{r_1}\right)}{2\pi L k_o} + \frac{\ln\left(\frac{r_3}{r_2}\right)}{2\pi L k_m} + \frac{1}{2\pi r_3 L h_g}} \quad (2.21)$$

where

$q$  = rate of heat transfer, W

$T_g$  = flue gas temperature, °C

$T_s$  = steam temperature, °C

$r_1$  = radius up to oxide-scale surface, m

$r_2$  = inner tube radius, m

$r_3$  = outer tube radius, m

$h_s$  = convection coefficient of steam, W/(m<sup>2</sup> °C)

$h_g$  = convection coefficient of flue gas, W/(m<sup>2</sup> °C)

$L$  = tube length, m

$k_o$  = thermal conductivity of oxide-scale, W/(m °C)

$k_m$  = thermal conductivity of tube metal, W/(m °C)

The efficiency in heat transfer from the flue gas into the water contained in the boiler tube is greatly influenced by the scale deposits that are present on the interior wall of the boiler tube. When the scale deposits are absent, the heat transfer is deemed smooth and there are no overheating issues on the exterior of the tube wall. However, the presence of scale deposits will insulate the tube wall from the cooling effect of water and thus reduces the efficiency of heat transfer and increases the tube metal temperature. The increase in the tube metal temperature causes overheating and hence promotes creep formation.

## 2.5.2 Stresses on the Boiler Tube

Major components in HRSG such as economizer, superheater and reheater tubes are operated under high internal steam pressure. When it is subjected to this pressure, three mutually perpendicular stresses will be set up. The stresses are identified as

longitudinal stress, radial stress and circumferential stress. Longitudinal stress or also known as axial stress is a stress that tends to change the length of the body. Radial stress on the other hand is a stress that acts at a direction normal to the curved plane. Circumferential stress or commonly known as hoop stress is a stress in resisting the bursting effect from the internal pressure.

Based on the failure analysis carried out by Rahman, Purbolaksono and Ahmad (2010), they had proposed a calculation to estimate the hoop stress developed on the tube. The proposed expression is presented in Equation 2.22.

$$\sigma_h = p \frac{r_i + \frac{t}{2}}{t} \quad (2.22)$$

where

$\sigma_h$  = hoop stress, MPa

$p$  = operational internal pressure, MPa

$r_i$  = inner radius of the tube, m

$t$  = wall thickness of the tube, m

This calculation of  $\sigma_h$  is used in this project to determine the lifetime of the tube by substituting it into the Larson-Miller Parameter equation. The Larson-Miller Parameter equation will be discussed further in the next subsection.

### 2.5.3 Larson-Miller Parameter

The life of a superheater tubes is an important datum that helps plant engineers to plan for tube replacements or schedule maintenance work (Ganapathy 2003). Therefore, it is crucial to estimate the life of the boiler tube so that any accidents due to premature failure can be mitigated.

A continuous increment in scale thickness over a span of service hours has been observed in the internal wall of the water tube in Purbolaksono et al. (2010)

research. As the scale thickness increases, the tube metal temperature increases too. Therefore, in order to predict the life of a boiler tube, the information on the oxide layer formation is necessary. Different materials' creep data are available in the form of Larson-Miller Parameter (LMP). This relates the rupture stress value to oxide-scale temperature,  $T$  in degree Rankine and the remnant life,  $t$  in hours (Ganapathy 2003) as shown in Equation 2.23.

$$LMP = (T + 460)(20 + \log t) \quad (2.23)$$

Every tube that is in operation possesses an LMP value which increases with time. In order to determine the remaining lifetime, the LMP value is obtained via the calculation of hoop stress,  $\sigma_h$ . It is to be noted that different tube materials has different LMP chart. The LMP chart for both T12 and T22 ferritic steels will be attached together in the Appendix A and Appendix B.

#### 2.5.4 Boiler Tube Strength

The strength of alloy steels measured in terms of hardness changes with service exposure in a time and temperature dependant manner, often describe by the LMP (Viswanathan 1993). The hardness of a material changes due to formation of carbide within the microstructure of the alloy steel.

The correlation between the hardness and LMP is obtained through several material aging experiments in the laboratory. Roberts et al. (1985) had developed a correlation function for nominal 2.25Cr-1Mo (T22) steel by employing 100 g load and Vickers indenter. The correlation expression is presented in Equation 2.24.

$$HV = 961.713 - (0.020669 \times LMP) \quad (2.24)$$

where

$HV$  = Hardness Vickers, HV

$LMP$  = Larson-Miller Parameter

On the other hand, two groups of researchers; Cane, Aplin and Brear (1985) and Askins et al. (1988) had develop a correlation expression on normalised and tempered 1Cr-0.5Mo (T12) steel using load ranging from 20 kg to 30 kg with Vickers indenter. The correlation is shown in Equation 2.25.

$$HV = 595.453 - (0.012605 \times LMP) \quad (2.25)$$

where

$HV$  = Hardness Vickers, HV

$LMP$  = Larson-Miller Parameter

The correlation expressions listed in Equation 2.24 and Equation 2.25 are adopted in this project to determine the behaviour in terms of tube strength for both T12 and T22 tube grades under several loading parameters.

## 2.6 Summary

To summarise as a whole, it is identified that one of the factor behind major tube failures is due to the waterside corrosion which causes scale deposition on the inner wall of the tube. The formation of the scales is caused by the high temperature chemical reaction between the treated boiler water and the tube materials. As the oxide-scale on the tube wall increases, it acts as a thermal barrier and an effective insulator causes slow heat transfer from the hot flue gas into the water contained in the tube, which indirectly increases the tube temperature. Increase in tube temperature results in a distorted microstructure and weak tube material strength which then results in creep formation on the exterior wall of the tube.

Another factor would be the fireside corrosion which leads to wall thinning of the tube. Thinning effect on the tube exterior wall is contributed by the chipping and erosion from the action of flying foreign matter in the hot flue gas. Moreover, the tube metal may also be consumed by the corrosion process due to the right chemical composition of flue gas. As the wall is thinned down to a certain limit, it could not

uphold the constant amount of pressure inside the tube. This causes a huge leap in hoop stress on the tube; to a certain limit above the maximum allowable stress where the tube started to enter its critical state upon yielding. As both of these effects combined, it fastens the creep rate and thus reduces the lifespan of the boiler tube.

From the above findings, it is important to always evaluate the wall thickness reduction and the oxide-scale formation in order to mitigate the unwanted breakdowns and accidents from occurring.

A simple one-dimensional model is developed in this project to evaluate the tube's behaviour which includes the effect of oxide-scale growth on the inner wall and wall thinning on the exterior wall of the tube. The evaluation is carried by incorporating most of the concepts and correlations discussed in this chapter into the iterative analytical program.

## **CHAPTER 3**

### **METHODOLOGY**

#### **3.1 Iterative Analytical Method in MATLAB**

As mentioned in the previous chapter, any rupture in the boiler tubes could result in subsequent damages to the boiler and possibly leads to life threatening scenarios. Therefore, it is important to maintain the boiler tubes in good condition. Any methods that can provide advanced warning of such failures are preferred as it allows immediate corrective actions to be carried out. Although there are many methods to predict possible failure occurrence such as visual testing, ultrasonic and other non-destructive testing, they are time consuming and expensive. Therefore, a simpler yet cost effective iterative analytical method is adopted in this project.

In this iterative analytical method, the performance of the boiler tube is evaluated by varying several key parameters, which includes the tube geometry, wall thinning effect and several other operation parameters. After going through the literature review to understand on how the development of oxide-scale, wall thinning and other concepts that affects performance of boiler tubes, the iterative analytical method is implemented into the MATLAB code. Figure 3.1 shows the simple flow chart of the iterative procedure in MATLAB.

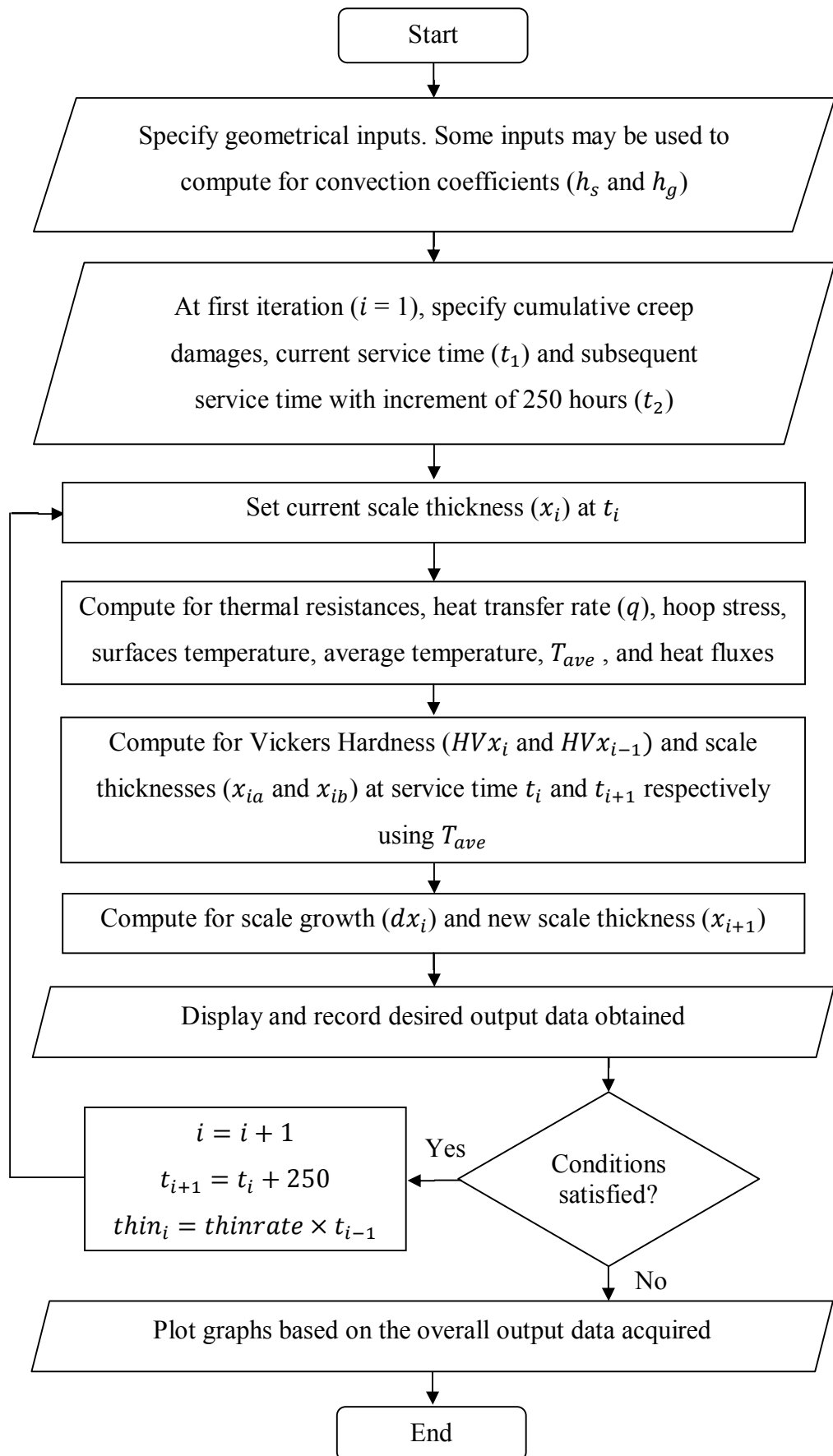


**Figure 3.1: Simple Flow Chart on the Analytical Procedure in MATLAB**

Firstly, user is prompted to key in all necessary geometrical inputs and boundary conditions. Geometrical inputs such as mass flow rate of steam, inner diameter of tube, steam temperature and steam pressure may be used to compute for convection coefficient of steam if it is not predetermined by the user beforehand. The same scenario applies if convection coefficient of flue gas is unknown. The geometrical inputs to determine the flue gas convection coefficient are flue gas temperature, flue gas compositions, gas flow rate, number of tube wide, transverse pitch, length and outer diameter of the tube. Both the convection values are solved by using the empirical formula proposed by Incropera et al. (2007) and Ganapathy (2003). Other geometrical inputs, for instance, LMP value, existing scale thickness in the tube, wall thinning rate and thermal conductivity for both oxide-scale and tube metal are stored in the MATLAB workspace for later use. A list of all the input geometries/parameters is tabulated in Table 3.1.

Next, at the first iteration ( $i = 1$ ), boundary conditions such as cumulative creep damages ( $CCDMG_1$  and  $CCDMG_2$ ) and initial thin thickness ( $thin$ ) due to wall thinning effect is set to zero. First service hour ( $t_1$ ) and increment of 250 hours as the second service hour ( $t_2$ ) are specified. The current scale thickness,  $x_1$  at  $t_1$  is determined based on the existing scale thickness input by the user.

Then, the MATLAB program solves for thermal resistances for each region ( $R_{steam}$ ,  $R_{oxide}$ ,  $R_{metal}$  and  $R_{gas}$ ) which is used to obtain radial heat transfer rate ( $q_{radial}$ ). In order to compute for the hoop stress value, the proposed calculation by Rahman et al. (2010) as discussed in the previous chapter is adopted. The temperature on the oxide-scale surface, oxide-metal interface surface and metal surface and its respective average temperatures ( $T_{ave_o}$  and  $T_{ave_m}$ ) are determined. Then, the heat flux on each surfaces are computed using the surface temperatures found previously.

Vickers Hardness ( $HV_{x_1}$  and  $HV_{x_2}$ ) are determined using the calculated  $T_{ave_m}$  at its respective service times ( $t_1$  and  $t_2$ ). At the same service hours, the scale thicknesses ( $x_{1a}$  and  $x_{1b}$ ) are computed. The difference between  $x_{1a}$  and  $x_{1b}$  is the

scale increment ( $dx_1$ ). The computation part of the program ends by finding the new scale thickness ( $x_2$ ).

All the desired output results from the program computations stored in the MATLAB workspace is then displayed in the MATLAB Command Window and recorded in output text (.txt) file. The program then decides whether all loop conditions has been satisfied. The two loop conditions specified in this program are:-

1. Current cumulative creep damage ( $CCDMG_2$ ) must be less than unity.
2. Current service hour must be less than 160000 hours as the analysis and evaluation in this project is only done up to 160000 hours.

If the two conditions stated above are satisfied, the next iteration ( $i = i + 1$ ) will increase its subsequent service hours by 250 hours ( $t_{i+1} = t_i + 250$ ). Besides, value of *thin* from the wall thinning effect will be considered for calculation in thermal resistances ( $R_{metal}$  and  $R_{gas}$ ) and hoop stress at latter part of the loop.

On the other hand, if any of the conditions is not fulfilled, the program will exit the loop and the desired graphs are plotted using the results stored in the MATLAB workspace. The program then ends here until user decides to run the program again.

There is one condition specified in the program that serves as the monitoring parameter on the tubes' status. The tube is said to have reached its critical state when the hoop stress exceeds the maximum allowable stress listed in Table 2.3.

Before the program was adopted in this project, Ang (2013) had tested and verified the program by comparing the results reported in Purbolaksono et al. (2009a). The outcome from the program showed an agreement with the author's published results. This shows that the program has the correct method of analysis, accurate and reliable.

### 3.2 Case A – Exponent Rate Comparison in Kinetic of Oxidation

The exponent rate between Rehn and Apblett (1981) for  $n = \frac{1}{3.0}$  and Dewitte and Stubbe (1986) for  $n = \frac{1}{2.0}$  for oxide-scale growth expression in ferritic tubing in Equation 2.1 were tested. This testing was necessary in order to determine the appropriate value of  $n$  and the growth-rate constant,  $k$  to represent the value of the oxidation behaviour in this project as observed from the experiment performed by Osgerby and Fry (2003).

MATLAB function files for this verification have been developed for each exponent rate. Two separate graphs; scale thickness versus service hour to the exponent values of  $\frac{1}{2.0}$  (or equivalent to 0.5) and  $\frac{1}{3.0}$  (or equivalent to 0.33) were plotted. The gradient for each plot were summed up to obtain the average growth-rate,  $\bar{k}$ . On the other hand, similar graphs were also plotted in Microsoft Office Excel (MS Excel) for both exponent rates using the output data recorded by MATLAB. The line expression ( $Y = kX$ ) was then generated on each plot in MS Excel in order to obtain the gradient,  $k$ .

The  $\bar{k}$  value obtained in MATLAB was then compared with  $k$  value obtained in MS Excel. This step was necessary in order to validate the method of averaging the  $\bar{k}$  value in MATLAB can approximately resembles the theoretical  $k$  value determined in MS Excel.

Meanwhile, the selection for best representation of  $n$  exponent was done through observation of “best fit” linear regression line using coefficient of  $R^2$  generated in MS Excel. The input parameters for this study were based on the models reported in the literature (Purbolaksono et al., 2009a) and will be presented later in Table 3.3. The models for this case were labelled alphabetically; for instance, Model A, Model B, Model C and so on.

### **3.3 Case B – Performance Analysis on Boiler Tubes**

In this project, parametric studies were conducted to determine the behaviour and performance of the boiler tube by using eight different models. From the eight models, Model 1, which was a similar model used in Kapar Power Station Malaysia as reported by Purbolaksono et al. (2009a), was used as a reference model for comparison to other seven models by varying key parameters required in the analysis. For instance, Model 2 has thicker tube thickness as compared to Model 1; Model 3 has higher flue gas temperature; Model 4 has slower steam mass flow rate; Model 5 has slower flue gas mass flow rate; while Model 6 has higher steam pressure. Model 7 was developed to study the wall thinning effect with the wall thinning rate of 0.00001817 mm/hr (Purbolaksono et al., 2009b). In order to study on the performance of two different tube grades, Model 8 was modelled as T12 grade material which has a lower Cr and Mo content than T22 grade used in Models 1 to Model 7.

The behaviour of the tube models in this project were observed through interpretation of the output data recorded by MATLAB as attached in Appendix C. Besides that, the comparisons between models were presented in graphical forms of average temperatures, scale thicknesses, oxide-scale growth, hardness, heat fluxes, stresses and creep damage.

### **3.4 List of Cases and Models**

The tables presented in this subsection show all the necessary input geometries/parameters and its respective variables that were used in the MATLAB program. They were arranged according to the case of study. The output results generated by MATLAB will be discussed further in the next chapter.

**Table 3.1: List of Input Geometries and Its Respective MATLAB Variables**

<i>Parameter</i>	<i>MATLAB Variable</i>
Flue Gas Composition	% CO2
	% H2O
	% N2
	% O2
	% SO2
	% HCl
Thermal conductivity of oxide-scale	ko
Thermal conductivity of tube metal	km
Number of tube wide	Nw
Transverse pitch	St
Tube outer diameter	do
Tube inner diameter	di
Tube length	l
Mass flow rate of steam	m_dot_s
Steam temperature	Ts
Steam pressure	pressure
Flue gas temperature	Tg
Larson Miller Parameter	LMP
Mass flow rate of flue gas	Wg
Initial oxide-scale thickness	thickness
Wall thinning rate	thinrate
Convection coefficient of steam	hs
Convection coefficient of flue gas	hg

**Table 3.2: Constant Parameters for Case A**

<i>MATLAB Variable</i>	<i>Unit</i>	<i>Value</i>
pressure	MPa	4
l	m	10
LMP	-	39.9
ko	W/m °C	0.592
km	W/m °C	34.606
thickness	m	0
thinrate	mm/hr	0

(Purbolaksono et al., 2009a. p. 899)

**Table 3.3: List of Models for Case A**

<i><b>MATLAB Variable</b></i>	hs	Ts	hg	Tg	di/2	do/2
<i><b>Unit</b></i>	W/m <sup>2</sup> °C	°C	W/m <sup>2</sup> °C	°C	m	m
<i><b>Model A</b></i>	2053.65	540	126.01	800	0.0219	0.0254
<i><b>Model B</b></i>	566.70	540	126.01	800	0.0219	0.0254
<i><b>Model C</b></i>	2053.65	540	130.96	900	0.0219	0.0254
<i><b>Model D</b></i>	2053.65	540	135.62	1000	0.0219	0.0254
<i><b>Model E</b></i>	2053.65	540	133.47	900	0.0219	0.0274
<i><b>Model F</b></i>	2440.00	540	130.96	900	0.0199	0.0254
<i><b>Model G</b></i>	2118.21	605	126.01	800	0.0219	0.0254

(Purbolaksono et al., 2009a. p. 899)

**Table 3.4: Constant Parameters for Case B**

<i><b>MATLAB Variable</b></i>	<i><b>Unit</b></i>	<i><b>Value</b></i>
% CO2	%	0.0829
% H2O	%	0.1817
% N2	%	0.7108
% O2	%	0.0246
% SO2	%	0
% HCl	%	0
ko	W/m °C	0.592
Nw	-	32
St	m	0.1016
l	m	10
di	m	0.0438
thickness	m	0
Ts	°C	540

**Table 3.5: List of Models for Case B**

<i><b>MATLAB Variable</b></i>	do	m_dot_s	pressure	Tg	LMP	Wg	km	thinrate
<i><b>Unit</b></i>	m	kg/h	MPa	°C	-	kg/h	W/m °C	mm/hr
<i><b>Model 1</b></i>	0.0508	3600	7.0	800	38.4	400000	34.606	0.00
<i><b>Model 2</b></i>	0.0528	3600	7.0	800	38.8	400000	34.606	0.00
<i><b>Model 3</b></i>	0.0508	3600	7.0	1000	38.4	400000	34.606	0.00
<i><b>Model 4</b></i>	0.0508	720	7.0	800	38.4	400000	34.606	0.00
<i><b>Model 5</b></i>	0.0508	3600	7.0	800	38.4	300000	34.606	0.00
<i><b>Model 6</b></i>	0.0508	3600	8.0	800	37.6	400000	34.606	0.00
<i><b>Model 7</b></i>	0.0508	3600	7.0	800	38.4	400000	34.606	0.00001817
<i><b>Model 8</b></i>	0.0508	3600	7.0	800	37.2	400000	35.000	0.00

### 3.5 Time Step Specification

The evaluation in this project was done based on the time step specified in Table 3.6. Therefore, all necessary graphs were constructed based on the mentioned time step.

**Table 3.6: Time Step in Iterative Procedure**

<i><b>Step</b></i>	<i><b>Time step (h)</b></i>
1	1
2	250
3	500
4	1000
5	2500
6	5000
7	10000
8	20000
9	40000
10	60000
11	80000
12	100000
13	120000
14	140000
15	160000

## CHAPTER 4

### RESULTS AND DISCUSSIONS

#### 4.1 Case A – Exponent Rate Comparison in Kinetic of Oxidation

The theoretical and analytical  $k$  values obtained from MS Excel and MATLAB respectively based on the original expression in Equation 2.1 was used to compute for the percentage error, which is given by the Equation 4.1.

$$\% \text{ Error} = \frac{|\text{MATLAB Value} - \text{MS Excel Value}|}{\text{MS Excel Value}} \quad (4.1)$$

Table 4.1 and Table 4.2 show the percentage error calculated between the average  $\bar{k}$  value obtained through MATLAB and the  $k$  value obtained using MS Excel for both exponent rates.

**Table 4.1: Percentage Error for Exponent Rate of  $n = 0.5$**

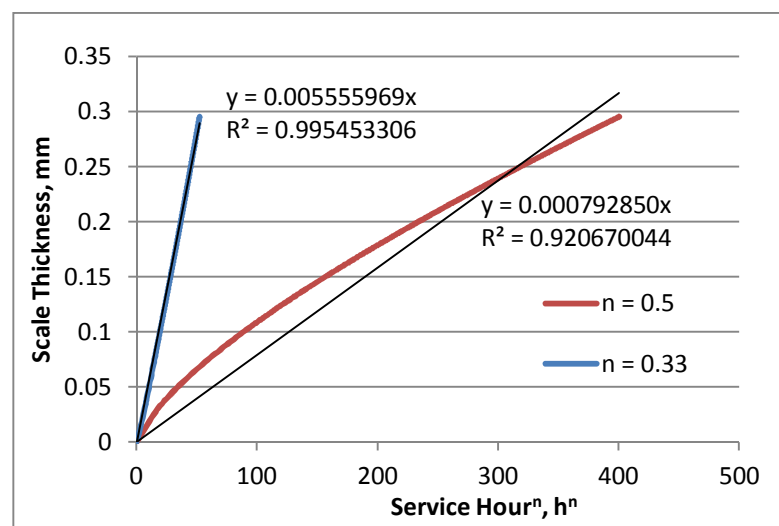
	$\bar{k}$ value from MATLAB	$k$ value from MS Excel	% Error
<b>Model A</b>	0.000856127	0.000792850	7.980951
<b>Model B</b>	0.002025785	0.001896823	6.798838
<b>Model C</b>	0.001057386	0.000989706	6.838393
<b>Model D</b>	0.001364581	0.001295864	5.302782
<b>Model E</b>	0.001121254	0.001052744	6.507762
<b>Model F</b>	0.001580498	0.001504657	5.040413
<b>Model G</b>	0.004405521	0.004196547	4.979666
		Average % Error	<b>6.206972</b>

**Table 4.2: Percentage Error for Exponent Rate of  $n = 0.33$** 

	$\bar{k}$ value from MATLAB	$k$ value from MS Excel	% Error
<i>Model A</i>	0.005492342	0.005555969	1.145194
<i>Model B</i>	0.012394134	0.012620116	1.790650
<i>Model C</i>	0.006803001	0.006928012	1.804427
<i>Model D</i>	0.008606821	0.008844293	2.685035
<i>Model E</i>	0.007219934	0.007366965	1.995812
<i>Model F</i>	0.008957880	0.009212538	2.764256
<i>Model G</i>	0.020791806	0.021337772	2.558682
		Average % Error	<b>2.106294</b>

From the results tabulated above, it can be observed that the exponent rate proposed by Rehn and Ablett (1981) yielded a deviation of about 2.1%. It was found to be more accurate than the percentage error computed from Dewitte and Stubbe (1986). Therefore, the method in determining  $\bar{k}$  value in MATLAB can be used for exponent rate of 0.33.

To identify which exponent rate curve could ‘best fit’ the linear regression line, a graph with correlation coefficient of  $R^2$  for both exponent rate for each models were plotted. When the value of  $R^2$  is close to unity, it shows a better line fit to the theoretical  $k$  value curve plotted by MS Excel. Graph for all the models are shown in Figure 4.1 to Figure 4.7.

**Figure 4.1: Scale Thickness versus Service hour<sup>n</sup> for Model A**

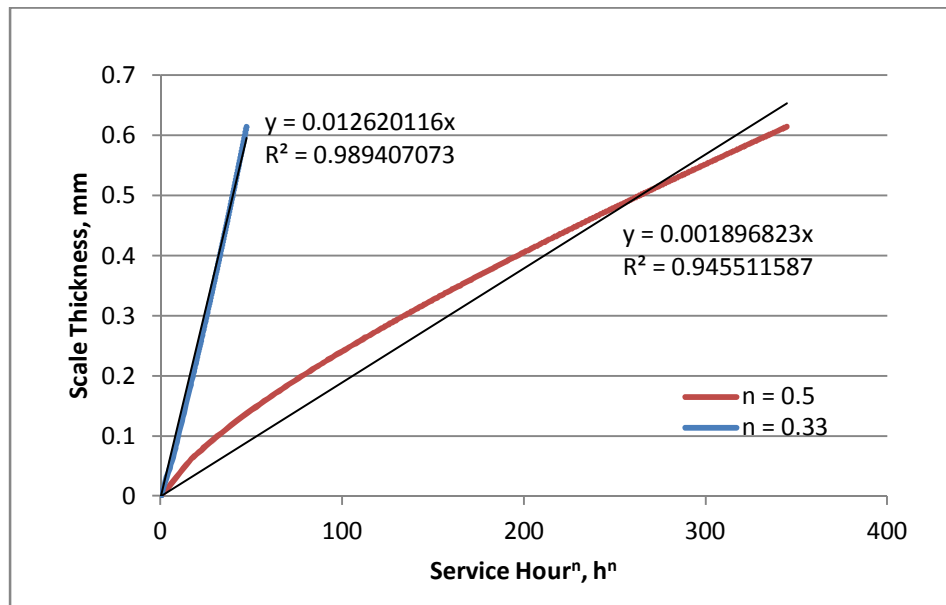


Figure 4.2: Scale Thickness versus Service hour<sup>n</sup> for Model B

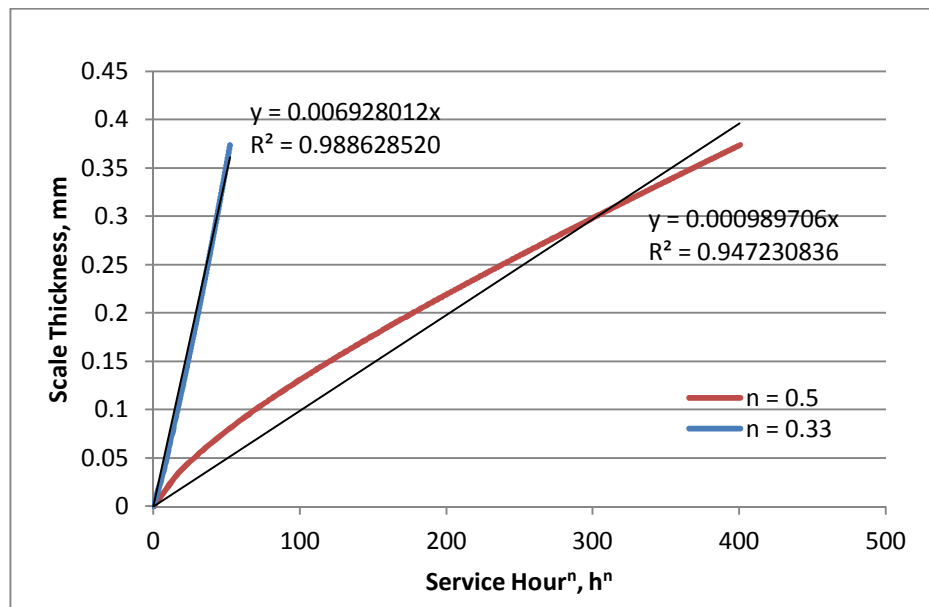


Figure 4.3: Scale Thickness versus Service hour<sup>n</sup> for Model C

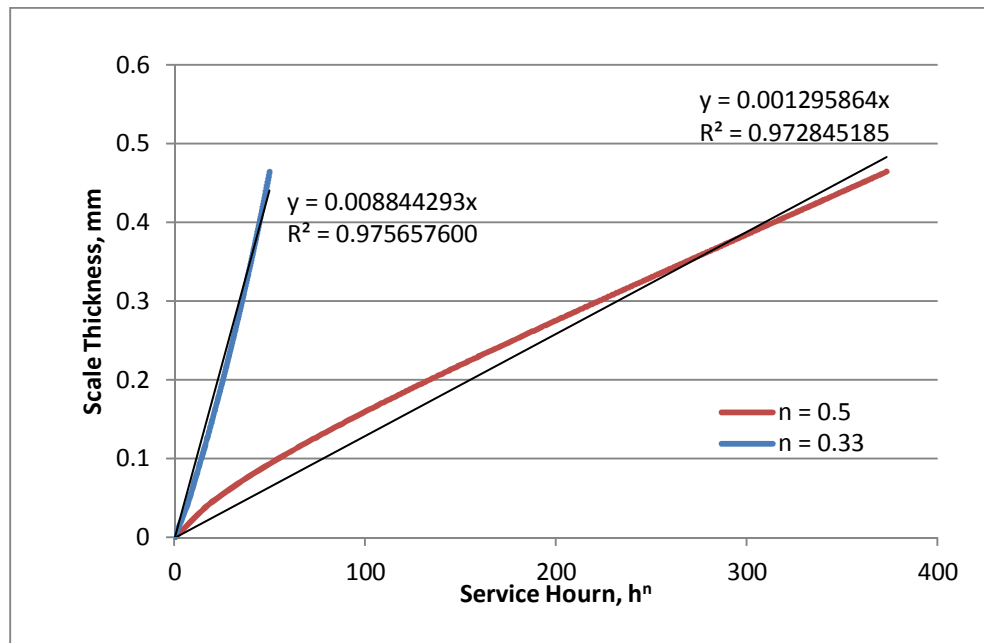


Figure 4.4: Scale Thickness versus Service hour<sup>n</sup> for Model D

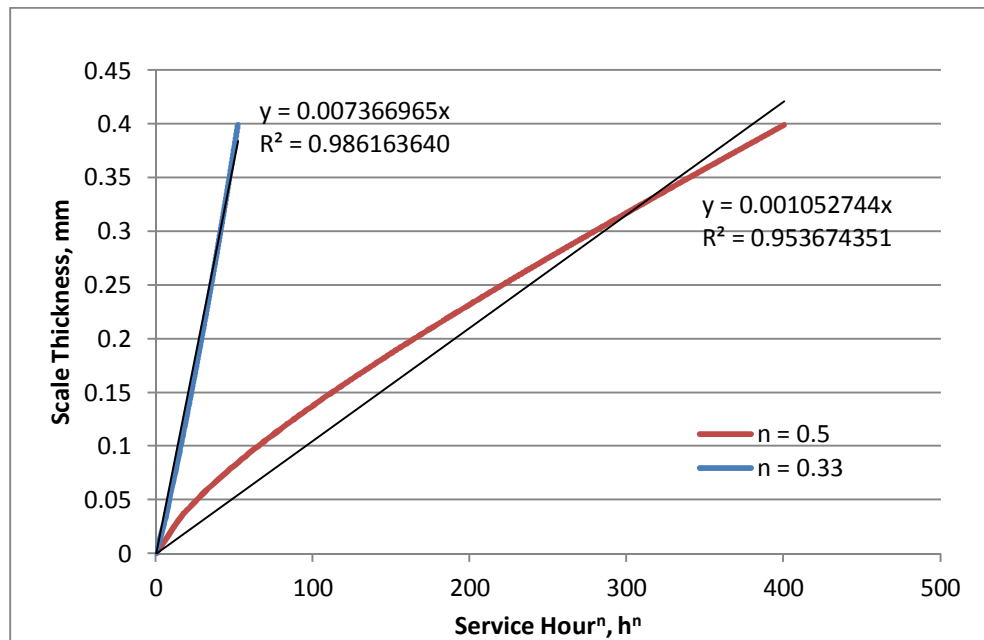


Figure 4.5: Scale Thickness versus Service hour<sup>n</sup> for Model E

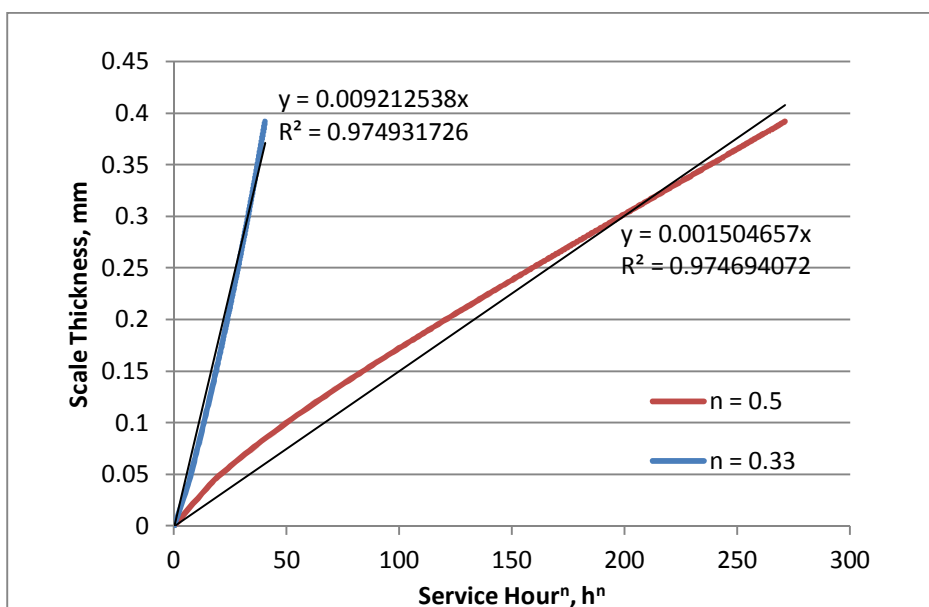


Figure 4.6: Scale Thickness versus Service hour<sup>n</sup> for Model F

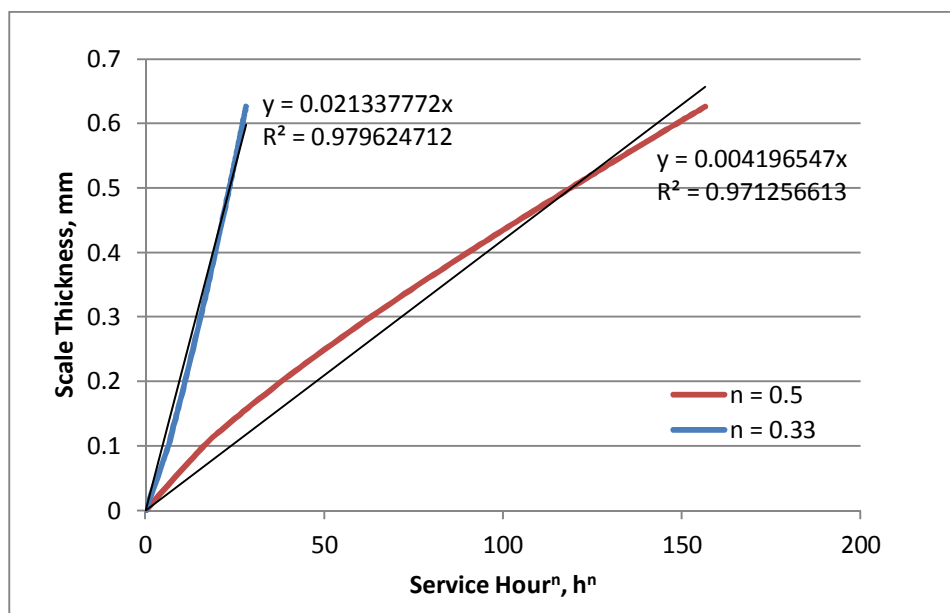


Figure 4.7: Scale Thickness versus Service hour<sup>n</sup> for Model G

According to the plots in Figure 4.1 to Figure 4.7, it was clear that the coefficient  $R^2$  has nearer value to unity for exponent rate of  $n = 0.33$  as compared to  $n = 0.5$ . This showed that  $n = 0.33$  has closer gradient value. Therefore, the value of  $n = 0.33$  has been selected in this project to determine the oxide-scale growth rate.

## 4.2 Case B – Performance Analysis on Boiler Tubes

Parametric studies have been conducted in this case to evaluate and analyse the performance of boiler tubes by changing seven key parameters with respect to the original model (Model 1). Some of the graphs presented in this section were plotted using MS Excel due to the limitation of MATLAB program in displaying proper comparison plots. The selected output data produced by MATLAB has been recorded and documented in the Appendix C for reference.

### 4.2.1 Effect of Tube Thickness

Model 1 and Model 2 were selected to study the effect of tube thickness on the performance of boiler tube. Figure 4.8 shows the hoop stress values for both models.

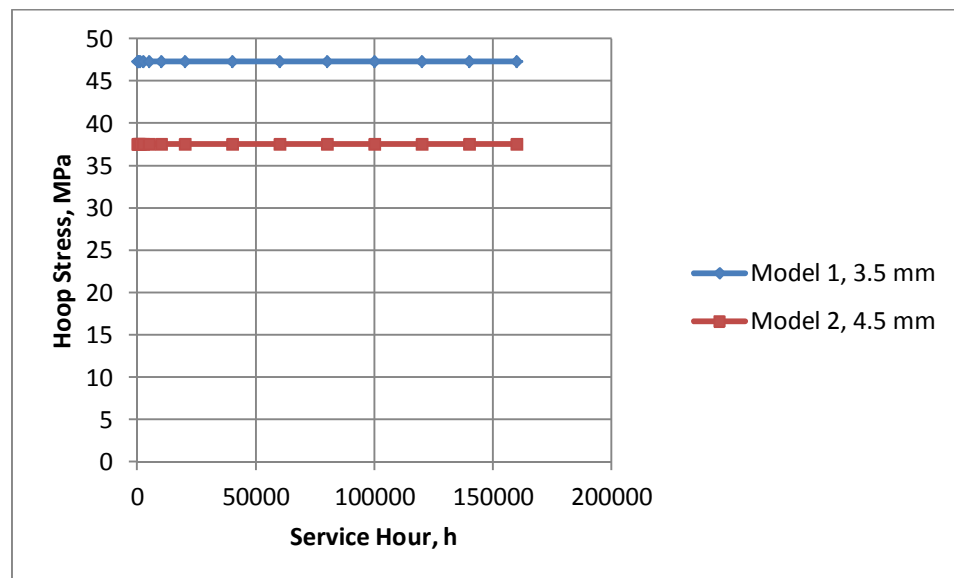


**Figure 4.8: Hoop Stress versus Service Hour for Model 1 and Model 2 with Different Tube Thickness**

In Figure 4.8, Model 2 which has a thicker tube thickness showed a lower operational hoop stress, a drop of about 20.58% as compared to Model 1. This observation was found to be true because based on Equation 2.22, the hoop stress is

inversely proportional to the tube thickness. Lower operational hoop stress in Model 2 resulted in a higher LMP value which resulted to a longer tube service life as shown in Figure 4.9.

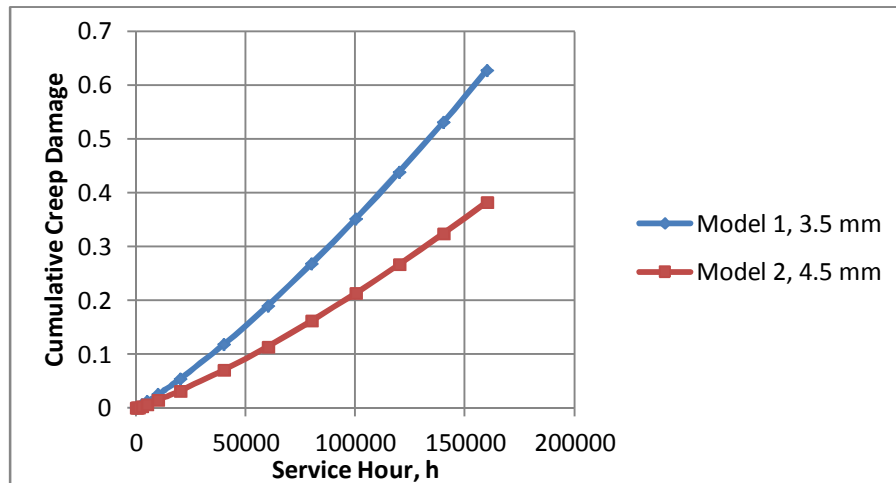


**Figure 4.9: Cumulative Creep Damage versus Service Hour for Model 1 and Model 2 with Different Tube Thickness**

Based on Figure 4.9, it was observed that both models were considered to have a life longer than 160000 hours because their creep lives have not reached unity. The rate of increase in creep damage for Model 1 was faster compared to Model 2. This implied that Model 1 could reach its creep life earlier than Model 2. One of the possible reasons for earlier creep life was due to the high operational hoop stress as discussed previously. Another possible reason for the early creep life in Model 1 was due to the early critical state tube as compared to Model 2. From Figure 4.10 and Figure 4.11, it can be seen that Model 1 has exceeded the maximum allowable stress limit and the tube has been operating in a critical state condition even before the start of operation (at 0<sup>th</sup> hour). On the other hand, Model 2 passed the maximum allowable stress limit after 97750 hours of service.

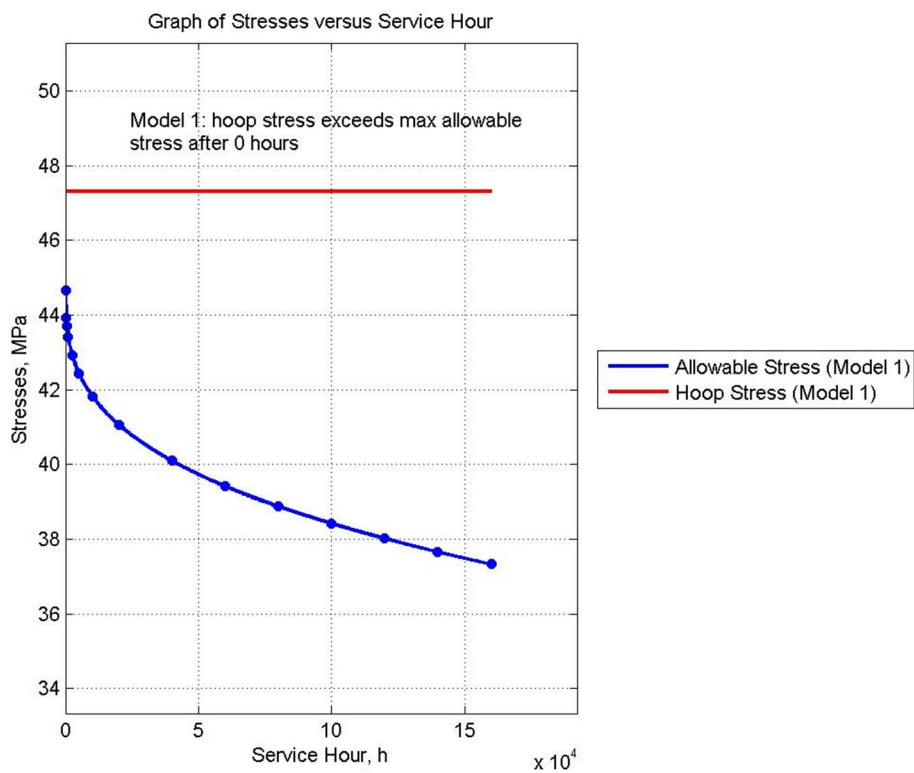


**Figure 4.10: Stresses versus Service Hour Plot for Model 1 for 3.5 mm thickness**

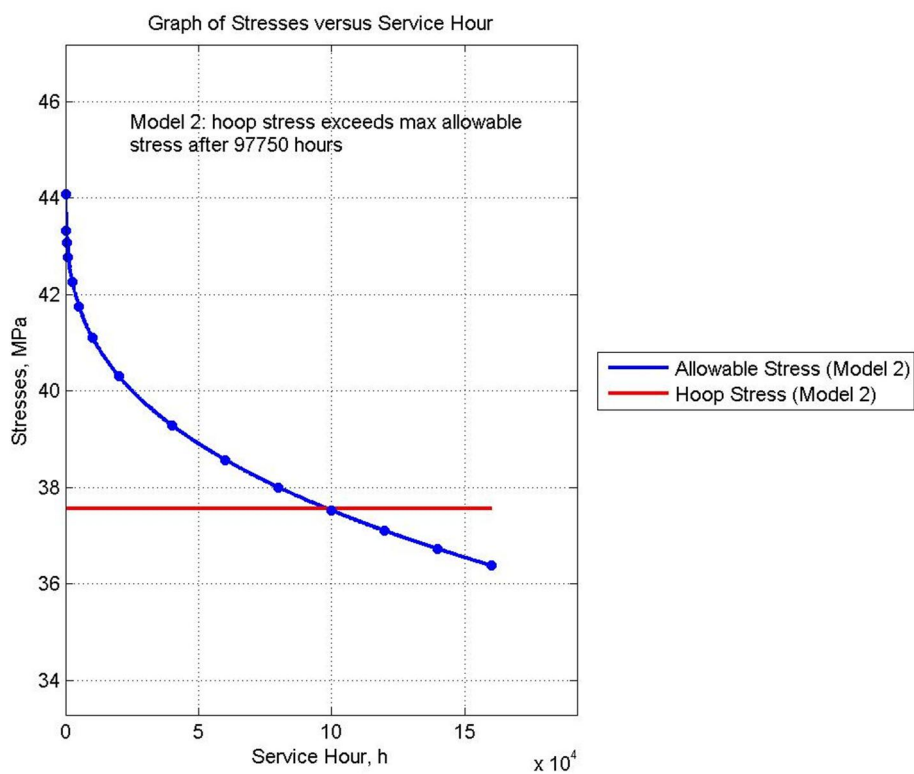


**Figure 4.11: Stresses versus Service Hour Plot for Model 2 for 4.5 mm thickness**

Therefore, a simple conclusion can be drawn whereby the tube's creep life is directly influenced by the operational hoop stress and the tube's condition (critical state or normal state). In other words, longer creep life can be achieved at lower hoop stress and with normal tube state.

#### 4.2.2 Effect of Flue Gas Temperature

The evaluation was continued by comparing Model 1 and Model 3, which have different flue gas temperature. Figure 4.12 shows the tube metal average temperature for both Model 1 and Model 3.

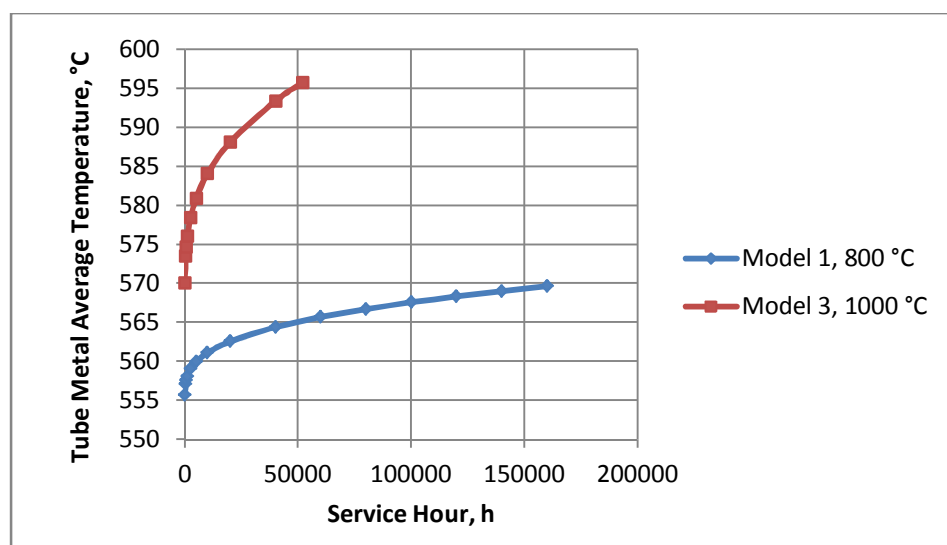


**Figure 4.12: Tube Metal Average Temperature versus Service Hour for Model 1 and Model 3 with Different Flue Gas Temperature**

From Figure 4.12, it can be identified that Model 3 operating with flue gas temperature of 1000 °C directly resulted in a higher tube metal temperature. Model 3 has a steeper climb in rate of increase in tube temperature as compared to Model 1. The constant exposure of the tube to high temperature resulted in long-term overheating as reported by EPRI (2007). The effect from long-term overheating caused some changes in the tube material microstructure. This effect will be discussed further in the next subsection.

As a consequence to the overheating, the tube failed due to creep rupture at shorter service hour as shown in Figure 4.13. The creep damage has reached its unity in Model 3 at about 110000 hours, or approximately 12.6 years earlier than Model 1.

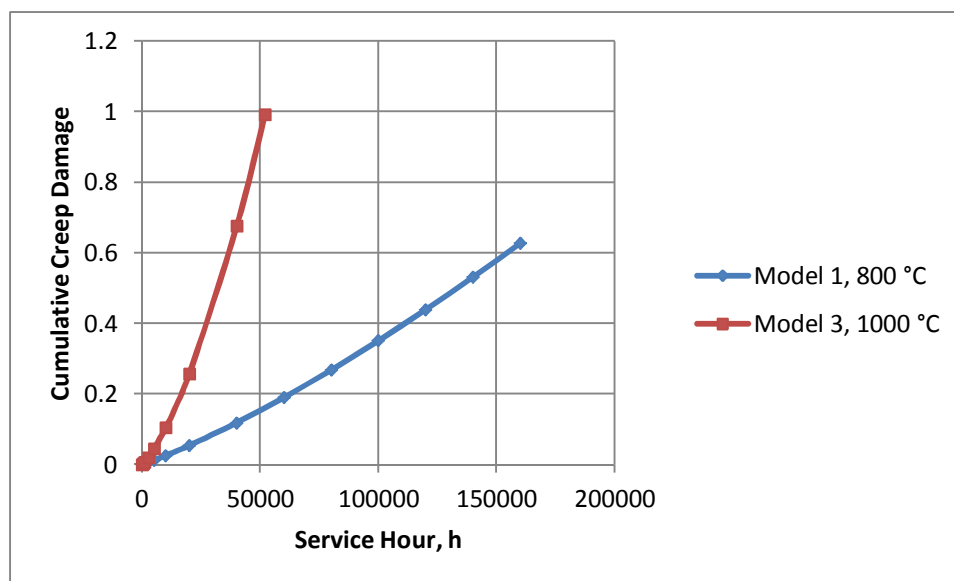


**Figure 4.13: Cumulative Creep Damage versus Service Hour for Model 1 and Model 3 with Different Flue Gas Temperature**

In summary, lower tube temperature due to lower flue gas temperature could result in a better creep life. Generally, the effect of tube metal average temperature is directly proportional to the creep damage.

### 4.2.3 Effect of Steam Mass Flow Rate

In this subsection, two models with different steam mass flow rate were evaluated. The results in terms of tube metal average temperature, scale thickness and hardness Vickers are presented in Figure 4.14, Figure 4.15 and Figure 4.16 respectively.



**Figure 4.14: Tube Metal Average Temperature versus Service Hour for Model 1 and Model 4 with Different Steam Mass Flow Rate**



**Figure 4.15: Scale Thickness versus Service Hour for Model 1 and Model 4 with Different Steam Mass Flow Rate**

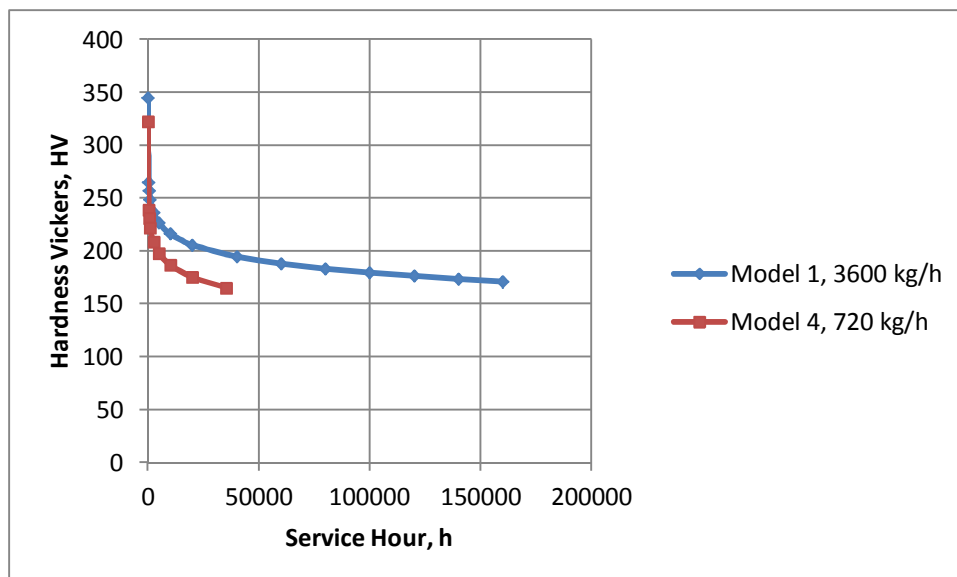


**Figure 4.16: Hardness Vickers Plot for Model 1 and Model 4 with Different Steam Mass Flow Rate**

Based on the plot in Figure 4.14, it can be observed that the tube metal average temperature for Model 4 was recorded to be 5.48 % higher than Model 1 when the steam mass flow rate was reduced. The main reason behind the increase in tube temperature was due to the decrease in steam mass flow rate which reduced the cooling effect on the tube metal. In other words, the slower steam flow could not completely dissipate the heat which was constantly induced by the flue gas. As it has been observed in the previous subsection, higher tube metal average temperature can result in shorter service hour due to potential failure of tube caused by creep damage. Therefore, Model 4 was expected to rupture earlier than Model 1.

From Figure 4.14 and Figure 4.15, it was noticed that the increase in the tube temperature was directly proportional to the oxide-scale thickness. Thick oxide-scale formed on inner wall of the boiler tube acted as an effective thermal barrier to heat transfer. As a result, the tube metal temperature increased. This forms a continuous cycle whereby the high tube metal temperature can accelerate the oxide-scale growth due to increase in acidity of boiler water at high temperature (Natarajan and Kumaresh 2006).

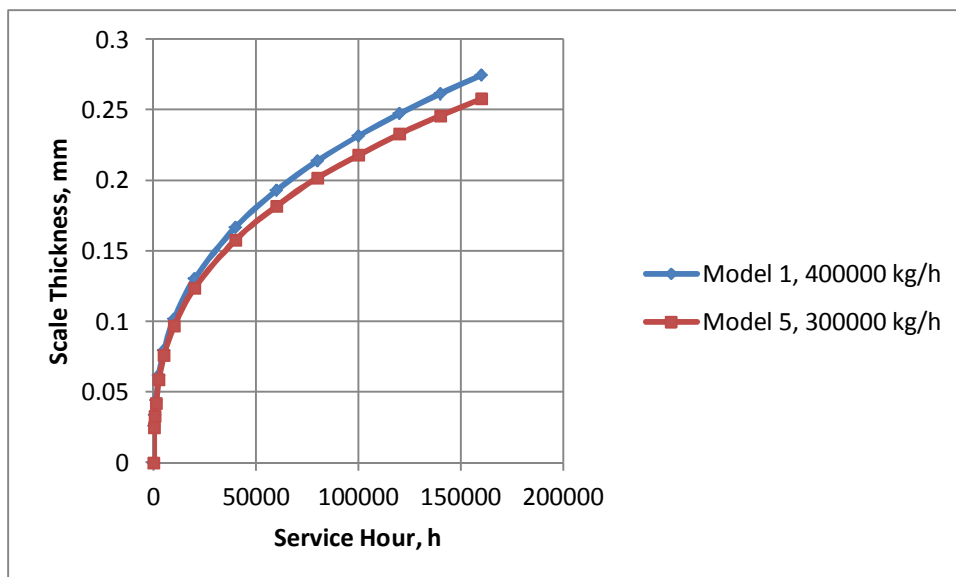
If the duration is prolonged, the scale thickness increases with increasing tube metal temperature until exfoliation occurs due to adhesion weakness on the boundary layers as reported by Jones (2004). When exfoliation occurred, blockage to steam passage which resulted in a lower mass flow rate of steam further accelerated the tube metal temperature to reach the overheating condition. As explained in the previous subsection, the overheating can lead to earlier creep life. Other effects on the tube average metal temperature due to scale thickness will be discussed in the next subsection.

Figure 4.14 and Figure 4.16 showed an inverse relationship between the tube temperature and hardness. Model 4 recorded lower hardness value as compared to Model 1. The reduction in hardness in Model 4 could be due to the elevated tube metal average temperature that caused formation of coarse carbide within the microstructure of the tube (Viswanathan 1993). The presence of carbides is undesirable because it can decompose to spheroidised carbides which are relatively soft. In order to avoid the formation of coarse carbide, it was recommended that the boiler tubes were to be operated within the design temperature.

To summarise as a whole, lower steam mass flow rate can result in higher tube temperature. The tube metal average temperature, oxide-scale thickness and its hardness value are inter-dependant on each other. Any increase in tube metal temperature, increase in scale thickness or reduction in the hardness can result in shorter life-span of the boiler tube.

#### **4.2.4 Effect of Mass Flow Rate of Flue Gas**

The effect from different flue gas mass flow rate was evaluated in this subsection. The results on scale thickness and kinetic of oxidation are plotted as shown in Figure 4.17 and Figure 4.18.



**Figure 4.17: Scale Thickness versus Service Hour for Model 1 and Model 5 with Different Flue Gas Mass Flow Rate**

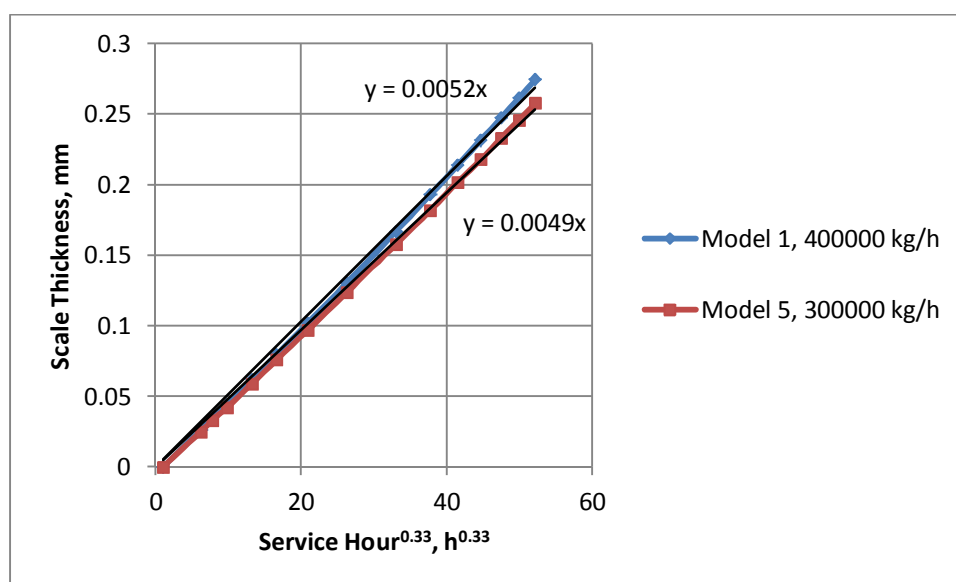


**Figure 4.18: Kinetic of Oxidation Plot for Model 1 and Model 5 with Different Flue Gas Mass Flow Rate**

In Figure 4.17, it was observed that the scale thickness for Model 5 has reduced compared to Model 1. There was also a reduction in the oxide-scale growth from  $0.0052 \text{ mm/hr}^{0.33}$  to  $0.0049 \text{ mm/hr}^{0.33}$  as shown in Figure 4.18. Since the tube metal temperature is proportional to the scale thickness, the reduction in scale

thickness in this evaluation indicated that the tube metal temperature has also decreased. Similar reasoning from the previous observation was also applied here. The slow flue gas flow rate across the tube reduced the rate of heat addition onto the tube. Due to the constant heat dissipation mechanism on the interior of the tube, the tube temperature was recorded to be lower compared to Model 1. The lower rate of heat addition from the flue gas to the tube surface can be seen through lower heat flux value recorded on the outer surface of the tube as shown in Figure 4.19.

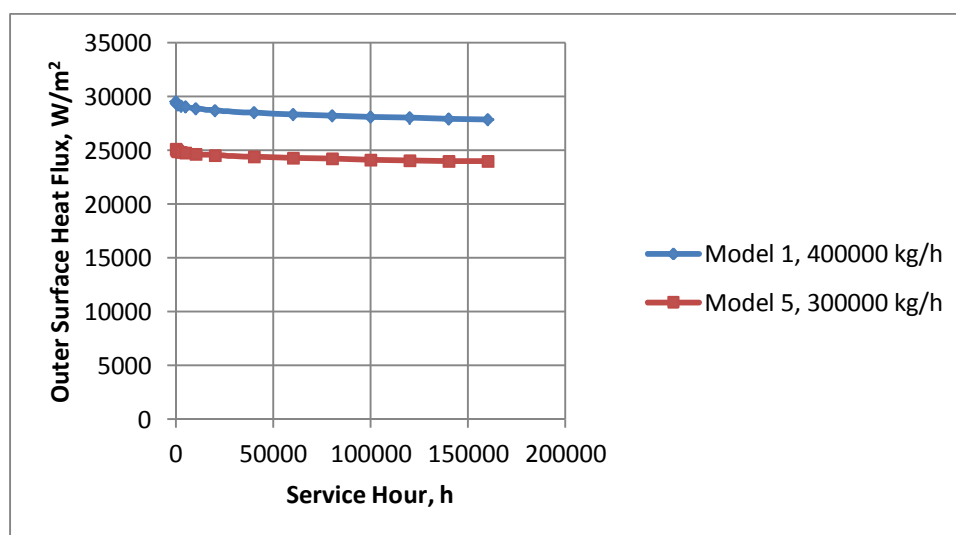


**Figure 4.19: Outer Tube Surface Heat Flux versus Service Hour for Model 1 and Model 5 with Different Flue Gas Mass Flow Rate**

Generally, the flue gas mass flow rate, oxide-scale thickness and its growth rate are proportional to the heat flux. A shorter creep life is expected when the heat flux increases.

#### 4.2.5 Effect of Steam Pressure

Based on the output data between Model 1 and Model 6 produced by MATLAB as shown in Appendix C, the most significant changes can be observed in terms of the operational hoop stress and its creep damage. The plots for both results are shown in Figure 4.20 and Figure 4.21.

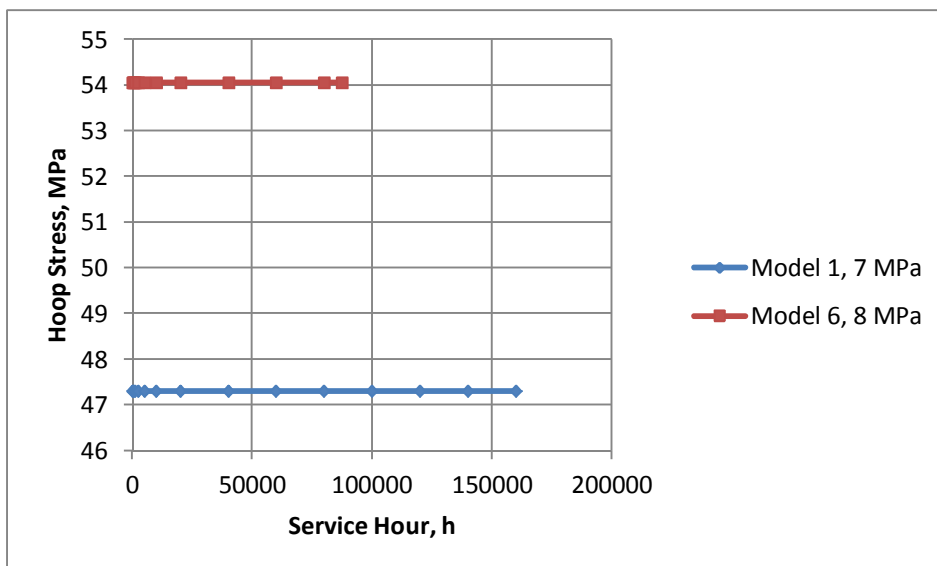


**Figure 4.20: Hoop Stress versus Service Hour for Model 1 and Model 6 with Different Steam Pressure**

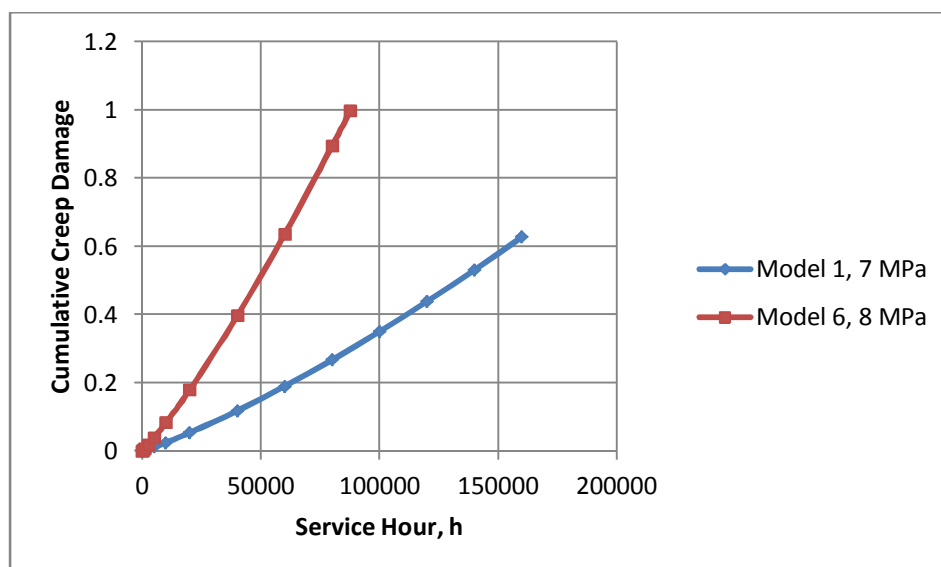


**Figure 4.21: Cumulative Creep Damage versus Service Hour for Model 1 and Model 6 with Different Steam Pressure**

From Figure 4.20, the increase of steam pressure by 1 MPa resulted in a jump of 14.29 % in hoop stress. The relationship between the hoop stress and steam pressure was given in Equation 2.22. As mentioned in the previous evaluation, the relationship between hoop stress and creep life of the boiler tube is inversely proportional to each other.

By observing the cumulative creep damage plot in Figure 4.21, Model 6 has an approximate service life of 87500 hours as the creep damage has reached its unity. When the hoop stress increases, the LMP value decreases and thus, decreases the service life of the boiler tube. Similar observation to Model 1 has been observed in Model 6 whereby the tube was in its critical state during its initial operation as shown in Figure 4.22.

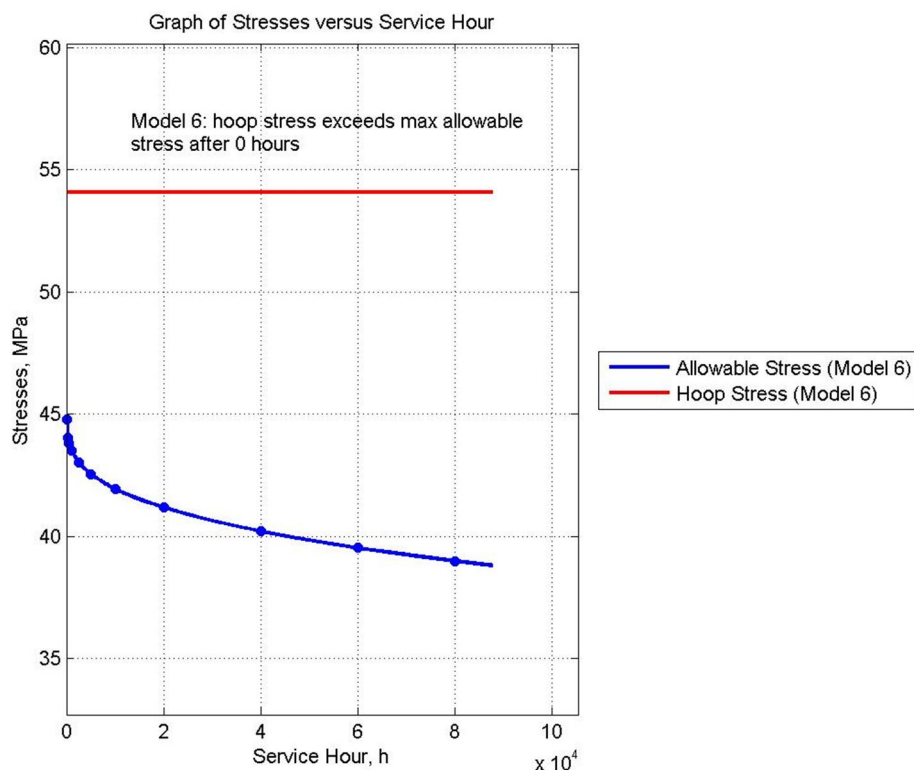


**Figure 4.22: Stresses versus Service Hour for Model 6 with Steam Pressure of 8 MPa**

In general, the evaluation in this section shows a direct proportional relationship between the steam pressure and its hoop stress. Similar conclusion in earlier study has been observed whereby the increase in hoop stress and the critical tube condition reduces the life span of boiler tube.

#### 4.2.6 Effect of Wall Thinning

An evaluation was conducted to compare on the effect of wall thinning towards the behaviour of boiler tube. Figure 4.23 shows the plot of hoop stress for both Model 1 and Model 7.

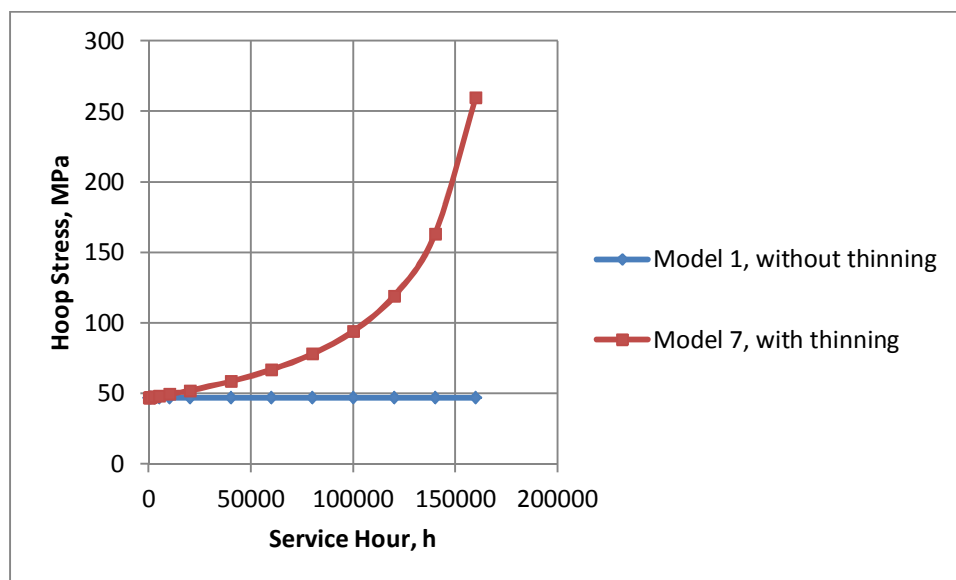


**Figure 4.23: Hoop Stress versus Service Hour for Wall Thinning Comparison between Model 1 and Model 7**

Based in Figure 4.23, can be observed that the behaviour of hoop stress was different compared to the other models observed previously. The hoop stress in Model 7 climbs exponentially until it reached to a value of approximately 260 MPa. The exponential behaviour was caused by the constant reduction of 0.00001817 mm in tube thickness per hour due to the wall thinning effect. Since the tube thickness and hoop stress has an inverse relationship, the higher hoop stress was developed. This relationship was found to be quite similar in Model 2. The only difference between Model 2 and Model 7 was the increase and decrease in tube thickness respectively.

From Figure 4.24, it can be seen that the Model 7 has been operating at critical state during its initial operation.

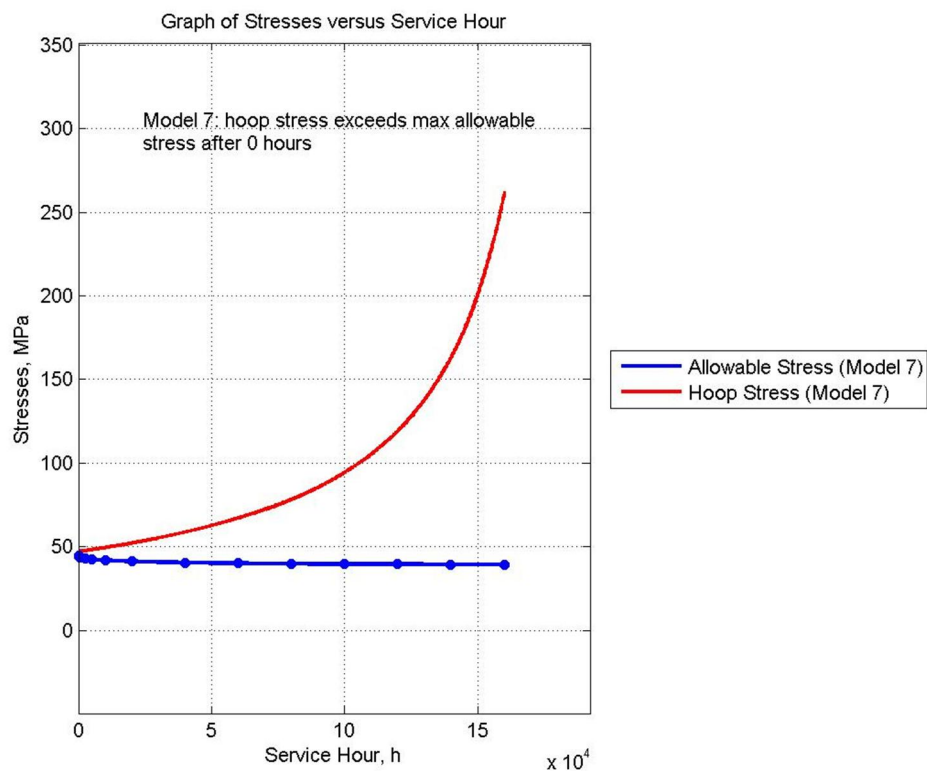


**Figure 4.24: Stresses versus Service Hour for Wall Thinning Effect in Model 7**

A further analysis was conducted in order to determine the minimum wall thickness required for Model 7 to be operating at a normal tube condition. Equation 2.3 was used for this analysis. During the initial operation (1<sup>st</sup> hour), the MATLAB has produced tube metal average temperature of 555.734 °C. The maximum allowable stress interpolated in Table 2.3 was found to be 44.672 MPa. By using the parameters listed in Table 3.5, the minimum wall thickness was computed to be 0.003945 m or 3.945 mm with an assumption that the tube was a strength welded type ( $e = 0$ ). The sample calculation has been demonstrated in Appendix D.

Based on Table 3.4 and 3.5, the initial tube thickness for Model 7 was calculated to be 0.0035 m or 3.5 mm. Therefore, it showed that Model 7 was operating at critical state during its initial operation.

Figure 4.25 shows the tube metal temperature for both Model 1 and Model 7. From the graph, it can be noticed that the rate of increase in temperature for Model 7 had slowed down. One possible reason for this phenomenon was due to the wall thinning effect had thinned down the tube material, thus reduced the thermal resistance to conduction which directly increased the efficiency of heat transfer from the flue gas into the steam. By applying the direct proportional relationship between scale thickness and tube temperature developed in previous evaluation, scale thickness in Model 7 was estimated to decrease in the same behaviour as the tube temperature.

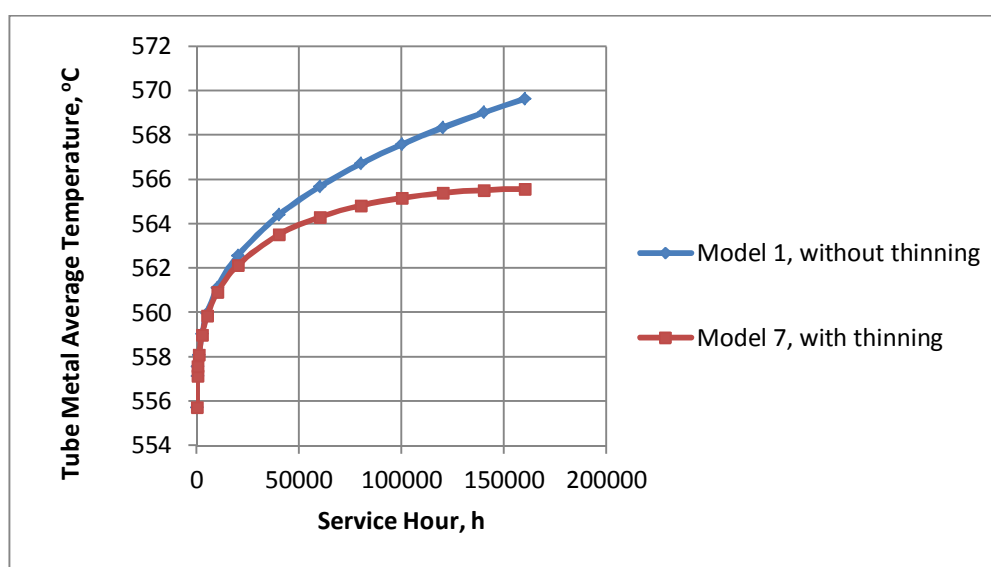


**Figure 4.25: Tube Metal Average Temperature for Wall Thinning Comparison between Model 1 and Model 7**

The cumulative creep damage graph for Model 7 could not be plotted directly due to the constant increase in hoop stress. Since the hoop stress is inversely proportional to the LMP value, the latter value need to be predetermined. Table 4.3 shows the data needed to plot the cumulative creep damage graph for Model 7. The cumulative creep damage comparison plot for both Model 1 and Model 7 were plotted as shown in Figure 4.26.

**Table 4.3: Some Output Results from MATLAB for Model 7 in Time Step. The Results is Used to Determine the LMP and CCDMG Values**

Time Step* (h)	Hoop Stress* (MPa)	Hoop Stress (ksi)	LMP**	Average. Tube Temp.* (°C)	CCDMG
1	47.300	6.860	37.8	555.734	0.00117
250	47.300	6.860	37.8	557.134	0.00246
500	47.357	6.869	37.8	557.558	0.00379
1000	47.471	6.885	37.8	558.089	0.00517
2500	47.818	6.935	37.8	558.992	0.00664
5000	48.407	7.021	37.8	559.861	0.00820
10000	49.635	7.199	37.6	560.912	0.01049
20000	52.304	7.586	37.4	562.147	0.01387
40000	58.689	8.512	37.0	563.514	0.02070
60000	66.996	9.717	36.4	564.311	0.03874
80000	78.246	11.349	35.6	564.828	0.10203
100000	94.342	13.683	35.0	565.172	0.16531
120000	119.273	17.299	33.8	565.394	0.22860
140000	163.064	23.650	32.4	565.524	1.28583

\* Results extracted from Model 7 in Appendix C

\*\* Values predetermined through LMP chart interpolation in Appendix B

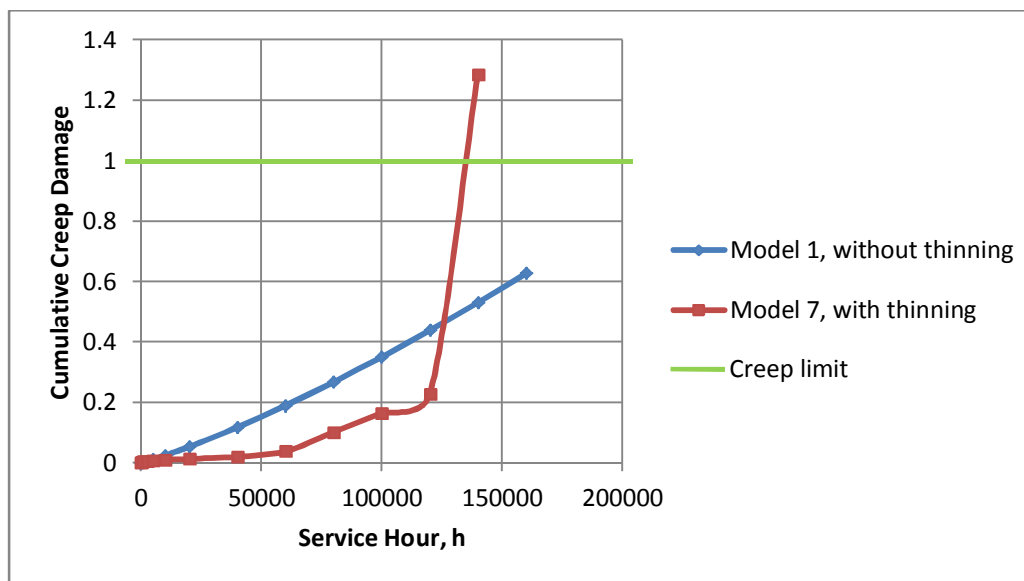


**Figure 4.26: Cumulative Creep Damage Plot for Wall Thinning Comparison between Model 1 and Model 7**

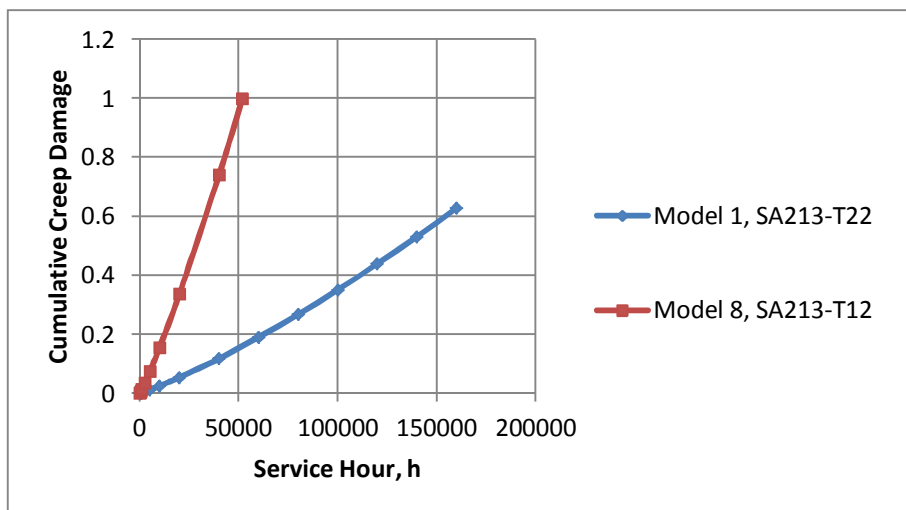
From Figure 4.26, it can be seen that at the early service hours, Model 1 has higher creep damage than Model 7. Starting from 60000<sup>th</sup> hours, the wall thinning effect has become significant to the increase in hoop stress which caused a drastic drop in LMP value. At approximately 125000<sup>th</sup> hour, the creep damage in Model 7 was recorded to be equivalent to the creep damage in Model 1. At last, Model 7 reached its creep life at approximately 130000<sup>th</sup> hour. This shows that the increase in hoop stress leads to a drastic increase in creep damage.

To conclude, the wall thinning effect causes a drastic increase in hoop stress level, thus decreases the creep life of the boiler tube. The tube metal temperature can be seen to be slowly decreases with time due to a better thermal conduction across a thinner tube.

#### **4.2.7 Effect of Tube Material with Different Cr and Mo Content**

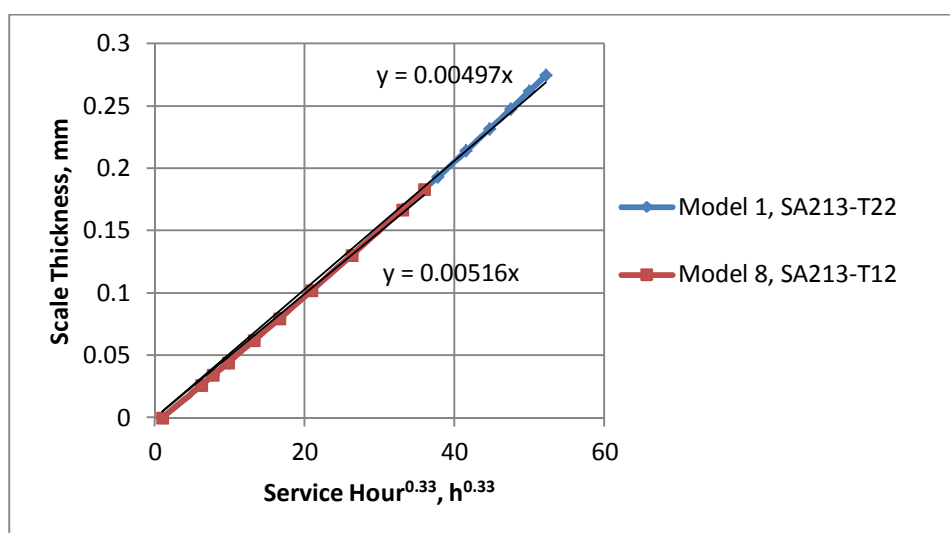
In this subsection, the performance between two tube grades; T12 and T22 were evaluated. Based on the nominal material composition for both T12 and T22 grade listed in Table 2.1, it can be observed that T22 has higher Mo and Cr content compared to T12. As stated in in Table 2.2, both Cr and Mo alloying elements' function are to increase the hardness, improves the creep strength at high temperature and to enhance the corrosion resistance. Therefore, the positive outcomes are anticipated in this evaluation based on the statements above.

Figure 4.27 shows the plot for cumulative creep damage for both Model 1 and Model 8. It can be observed that Model 8 failed at around 50000 hours due to unity in creep life. From the table in the Appendix C, it can be seen that both hoop stress and tube metal temperature appeared to be the approximately same. Therefore, the hoop stress and tube metal temperature relationship as observed from the previous models were invalid for this case. One possible reason that caused a better creep life in Model 1 was the higher LMP value as observed in Table 3.5. Due to the difference in tube grade, two different LMP charts were used to determine the LMP value at the same hoop stress. Those charts can be accessed in the Appendix section.



**Figure 4.27: Cumulative Creep Damage Plot for Tube Material Comparison between Model 1 and Model 8**

Figure 4.28 represents the rate of oxide-scale growth in both Model 1 and Model 8. Through direct comparison on the line of curve in Figure 4.28 and the scale thickness values recorded in table attached in Appendix C, there was no significant difference observed. When the line expression was generated and shown in the plot, Model 1 displayed oxide-scale growth rate of  $0.00497 \text{ mm/hr}^{0.33}$  as compared to the growth rate of  $0.00516 \text{ mm/hr}^{0.33}$  in Model 8. This shows that the oxide-scale was developed at a slower pace in Model 1 as compared to Model 8.



**Figure 4.28: Kinetic Oxidation Plot for Tube Material Comparison between Model 1 and Model 8**

Figure 4.9 shows the hardness plot for both Model 1 and Model 8. It can be identified that Model 1 has a higher hardness compared to Model 8. This was due to the different correlation expression used to represent different tube material. The correlation expression used for Model 1 and Model 8 are based on Equation 2.24 and Equation 2.25 respectively. Those correlation expressions were developed by a few group of researchers through several experiments conducted in the laboratory using different load and a Vickers indenter.



**Figure 4.29: Hardness Plot for Tube Material Comparison between Model 1 and Model 8**

As a conclusion, it can be learnt that tube grade T22 is a better material as it has a better corrosion resistance, higher creep strength and better tube strength than T12 material.

#### 4.2.8 Summary of Case B

As an overall summary in this case, it was observed that there were three major factors that could result in a shorter tube life.

One of the factors was the hoop stress and the tube's condition. Thinner tube geometry, higher steam pressure and the presence of wall thinning effect were observed to be the key parameters that could result in a higher hoop stress and critical tube condition. Critical tube state can be observed when the hoop stress exceeded the maximum allowable stress. The inverse relationship between the hoop stress and LMP value led to shorter creep life.

Besides that, the increase in average temperature of the boiler tube has been observed as one of the main factor that reduced the tube life. Other contributing factors to the increase in tube temperature have been identified, for instance, thick oxide-scale, fast oxide-scale growth rate, high surface heat flux and reduction in hardness. These contributing factors were caused by the direct influence of several key parameters such as low steam mass flow rate, high flue gas temperature and flow rate and thick tube geometry.

The last factor that could possibly lead to early tube rupture was the use of poorer tube grade. High tube grade material which contains higher amount of Cr and Mo alloying elements could prolong the tube life as it has better mechanical properties to withstand high operating temperature and pressure.

## **CHAPTER 5**

### **CONCLUSIONS AND RECOMMENDATIONS**

#### **5.1 Conclusions**

The parametric evaluation of the boiler tube based on several tube models have been presented in this project. An iterative analytical program has been adopted to determine the behaviour and performance of two different tube grades which accounts for several varying key parameters such as tube geometry, wall thinning effect and other input parameters towards the life of the boiler tube. Several conclusions have been drawn based on the studies conducted.

Based on the output results for all the cases, it was observed that factors such as scale thickness, rate of oxide-scale growth and the surface heat flux were directly proportional to the tube metal average temperature. An increase in these factors was due to low steam mass flow rate, high flue gas temperature and mass flow rate and thick tube geometry. Besides that, tube strength in terms of hardness was affected by the microstructural changes, in which it was inversely proportional to the tube metal average temperature. Overheated tubes operating at elevated temperature; for instance, temperature exceeding the maximum design temperature was observed to cause microstructural changes in the tube. Moreover, the increase in hoop stress contributed by the wall thinning effect resulted in an early tube rupture due to rapid climb in the creep damage. Other factor that could cause an increase in hoop stress has been identified to be higher steam pressure and thinner tube geometry. The comparison of two different tube grades; T12 and T22 showed that the latter material was a much better choice in terms of durability and reliability due to better creep

strength, material hardness and corrosion resistance as a result of increase in Cr and Mo composition in the tube.

## **5.2 Recommendations**

In order to increase the efficiency of power generation, most of the power plants opt for higher quality superheated steam, which can be produced by increasing the operating conditions. Since boiler tube life is greatly dependant to its tube temperature, it is suggested that constant monitoring should be carried out on the flue gas temperature. This is to ensure that the boiler could operate within the recommended manufacturer design temperature. This precaution step is necessary to reduce the possibility of overheated tubes from occurring which may accelerate the oxide-scale growth and creep rate.

Besides that, the increase in the loading conditions to achieve better steam quality may accelerate the wall thinning on the tube. Therefore, it is important to operate the boiler within the recommended optimum range specified by the manufacturer in order to attain both high quality steam and a shorter boiler maintenance interval. Operating the boiler above the design specifications will result in frequent maintenance, thus incurring more maintenance cost and downtime per year of operation.

A boiler typically operates at a fluctuating trend due to uncertain demand from consumers. Therefore, the boiler tubes may also experience cyclic thermal stresses due to metal expansion and contraction which leads to fatigue failure. Since boiler tubes are also exposed to elevated temperature, the combined effect of both creep and fatigue failure; termed as creep-fatigue interaction can be studied in the future project. The program can be expanded to include this interaction to estimate the remaining life of the boiler tube.

Besides that, several improvements can also be done on the program. One of them is to expand the program to include the minimum wall thickness criteria which

serves as a tube monitoring conditions side-by-side with the maximum allowable stress criteria. In future, this program can also incorporate another stopping criterion which is the yield strength of the tube material. Besides, a more user-friendly interface can be implemented to ease the user in graph plotting selection.

## REFERENCES

- Ang, W. B., 2013. Development of Iterative Analytical Procedure for Boiler Tube Analysis in MATLAB. Unpublished Final Year Project, Universiti Tunku Abdul Rahman. Malaysia.
- Askins, M. C. et al., 1988. *Remaining Life of Boiler Pressure Parts-Base Material Model*. Report RP 2253-1, Electric Power Research Institute. California, CA: EPRI.
- ASME, 2004a. *Section I – Rules for Construction of Power Boilers*. ASME Boiler & Pressure Vessel Code. New York, NY: The American Society of Mechanical Engineers.
- ASME, 2004b. *Section II Part D - Material Properties*. ASME Boiler & Pressure Vessel Code. New York, NY: The American Society of Mechanical Engineers.
- ASM International, 2002. *Introduction to Steels and Cast Irons - Metallographer's Guide: Irons and Steels (#06040G)*. Ohio: ASM International.
- Awassada, P., Changkook, R., Yao, B. Y., Karen, N. F., Adrian, L., Vida, N. S. and Jim, S., 2010. Investigation into high-temperature corrosion in a large-scale municipal waste-to-energy plant. *Corrosion Science*, 52, pp. 3861–3874.
- Cane, B. J., Aplin, P. F. and Brear J. M., 1985. A Mechanistic Approach to Remanent Creep Life Assessment of Low Alloy Ferritic Components Based on Hardness Measurements. *J. Pressure Vessel Technol.*, Vol. 107 (No. 3), pp. 295.
- Chandra, K., Kain, V. and Dey, G. K., 2011. Failure of 2.25Cr-1Mo steel superheater tubes in a fluidized bed combustor due to fireside corrosion. *Materials Characterization*, 62, pp. 62–69.
- Dewitte, M. and Stubbe, J., 1986. Personal communication to Roberts, D. A. of G. A. Technologies, San Diego from Laborolec Company, Belgium.
- EPRI, 2007. *Guidelines for the Nondestructive Examination of Heat Recovery Steam Generators*. California, CA: Electric Power Research Institute.

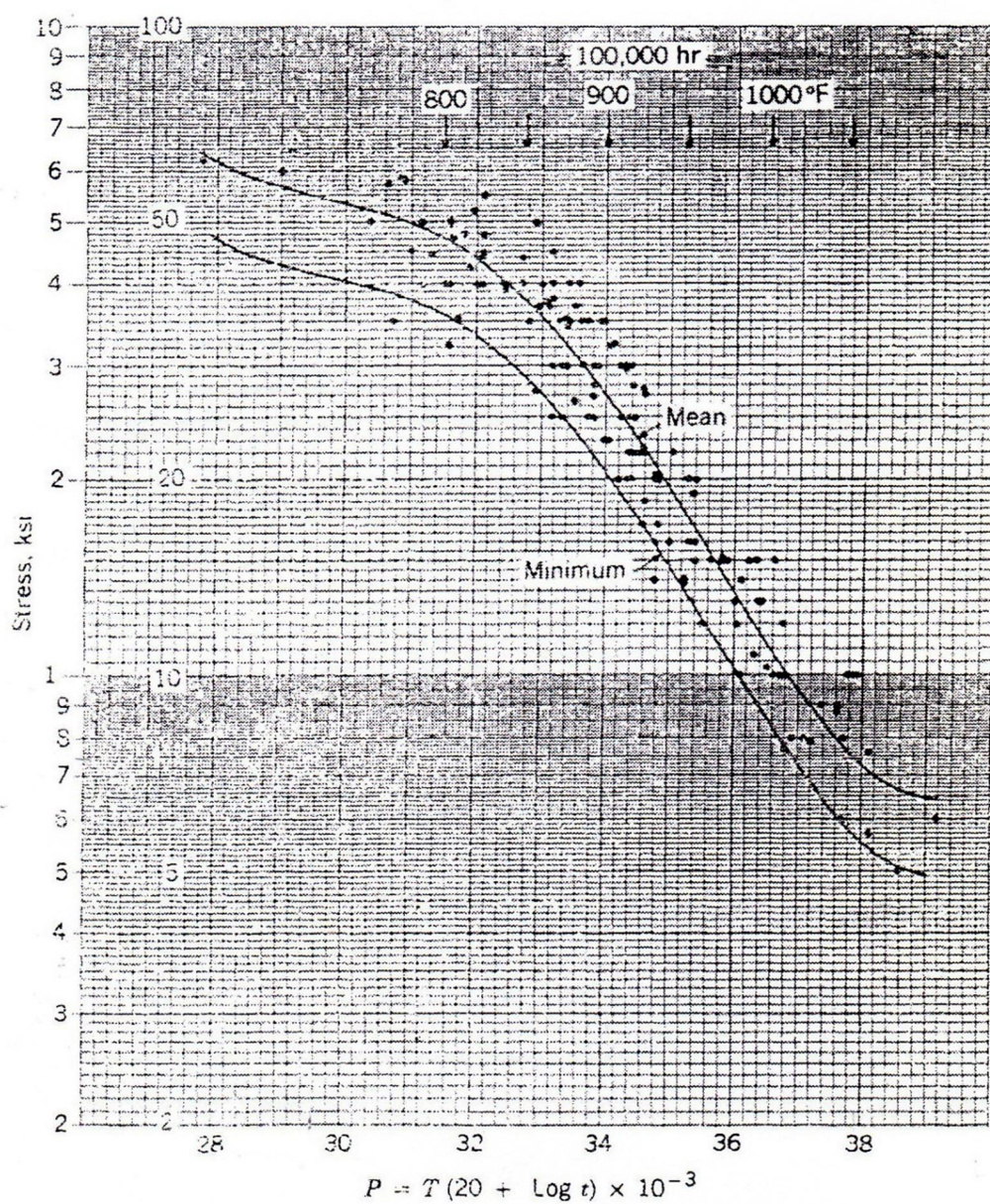
- Fry, A., Adams, B., Davis, K., Swensen, D., Munson, S. and Cox, W., 2011. An investigation into the likely impact of oxy-coal retrofit on fire-side corrosion behaviour in utility boilers. *International Journal of Greenhouse Gas Control*, 5S, pp. S179–S185.
- Ganapathy, V., 1994. *Steam Plant Calculations Manual*. 2nd ed. New York, NY: Marcel Dekker Inc..
- Ganapathy, V., 2003. *Industrial Boilers and Heat Recovery Steam Generators*. New York, NY: Marcel Dekker Inc..
- Hernas, A., Imosa, M., Formanek, B. and Cizner, J., 2004. High-temperature chlorine-sulfur corrosion of heat-resisting steels. *Journal Materials Processing Technology*, 157-158, pp. 348–353.
- Incropera, F. P., Dewitt, D. P., Bergman, T. L. and Lavine, A. S., 2007. *Fundamentals of Heat and Mass Transfer*. 7th ed. New Jersey, NJ: John Wiley & Sons.
- Jones, D. R. H., 2004. Creep failures of overheated boiler, superheater and reformer tubes. *Engineering Failure Analysis*, 11, pp. 873–893.
- Khajavi, M. R., Abdolmaleki, A. R., Adibi, N. and Mirfendereski, S., 2007. Failure analysis of bank front boiler tubes. *Materials Science and Engineering*, A432, pp. 47–51.
- Lee, N. H., Kim, S., Choe, B. H., Yoon, K. B. and Kwon, D. I., 2009. Failure analysis of a boiler tube in USC coal power plant. *Engineering Failure Analysis*, 16, pp. 2031–2035.
- Majidian, A. and Saidi, M. H., 2007. Comparison of Fuzzy logic and Neural Network in life prediction of boiler tubes. *International Journal of Fatigue*, 29, pp. 489–498.
- Moles, M. D. C. and Westwood, H. J., 1982. *Residual Life Estimation of High Temperature Superheater and Reheater Tubing*. Report CEA RP 78-66, Final Report of Ohio Hydro Research Division, Toronto, for Canadian Electrical Assn., Montreal, pp. 67-82.
- Mukhopadhyay, N. K., Dutta, B. K., Kushwaha, H. S., Mahajan, S. C. and Kakodkar, A., 1999. Implementation of finite element based fatigue monitoring system at Heavy Water Plant Kota. *Nuclear Engineering and Design*, 187(2), pp. 153–163.
- Mukhopadhyay, N. K., Dutta, B. K. and Kushwaha, H. S., 2001. On-line fatigue–creep monitoring system for high-temperature components of power plants. *International Journal of Fatigue*, 23, pp. 549–560.

- Natarajan, S. and Kumares, B. S. P., 2006. Corrosion and its inhibition in SA213-T22 TIG weldments used in power plants under neutral and alkaline environments. *Engineering Failure Analysis*, 14, pp. 731–738.
- Osgerby, S. and Fry, A., 2003. Personal communication. Simulating Steam Oxidation of High Temperature Plant under Laboratory Conditions: Practice and Interpretation of Data, NPL, United Kingdom.
- Purbolaksono, J., Khinani, A., Ali, A. A., Rashid, A. Z. and Nordin, N. F., 2009a. Iterative technique and finite element simulation for supplemental condition monitoring of water-tube boiler. *Simulation Modelling Practice and Theory*, 17, pp. 897–910.
- Purbolaksono, J., Tarlochan, F., and Rahman, M. M., Nordin, N. F. and Ahmad, B., 2009b. Failure Investigation on Reheater Tube Due to Deposit and Wall Thinning. *Journal of Failure Analysis and Prevention*, 9, pp. 365-369.
- Purbolaksono, J., Khinani, A., Rashid, A. Z., Ali, A. A. and Nordin, N. F., 2009c. Prediction of oxide scale growth in superheater and reheater tubes. *Corrosion Science*, 51, pp. 1022–1029.
- Purbolaksono, J., Khinani, A., Rashid, A. Z., Ali, A. A., Ahmad, J. and Nordin, N. F., 2009d. A new method for estimating heat flux in superheater and reheater tubes. *Nuclear Engineering and Design*, 239, pp. 1879–1884.
- Purbolaksono, J., Ahmad, J., Khinani, A., Ali, A. A. and Rashid, A. Z., 2010. Failure case studies of SA213-T22 steel tubes of boiler through computer simulations. *Journal of Loss Prevention in the Process Industries*, 23, pp. 98–105.
- Rahman, M. M., Purbolaksono, J. and Ahmad, J., 2010. Root cause failure analysis of a division wall superheater tube of a coal-fired power station. *Engineering Failure Analysis*, 17, pp. 1490–1494.
- Rahmani, A., Bouchami, T., Bélaïd, S., Salah, A. B. and Boulheouchat, M. H., 2009. Assessment of boiler tubes overheating mechanisms during a postulated loss of feedwater accident. *Applied Thermal Engineering*, 29, pp. 501–508.
- Ranjbar, K., 2007. Failure analysis of boiler cold and hot reheater tubes. *Engineering Failure Analysis*, 14, pp. 620–625.
- Rehn, I. M. and Apblett, W., 1981. *Corrosion Problems in Coal Fired Fossil Boiler Superheater and Reheater Tubes*. Report CS 1811, Electric Power Research Institute. California, CA: EPRI.
- Robert, D. P. and Harvey, M. H., 1991. *The Nalco Guide to Boiler Failure Analysis*. United States of America: McGraw-Hill Inc..

- Roberts, D. I. et al., 1985. *Dissimilar-Weld Failure Analysis and Development Program – Vol. 2 Metallurgical Characteristics*. Report CS 4252, Electric Power Research Institute. California, CA: EPRI.
- Robinson, E. L., 1938. Effect of the temperature variation on the creep strength of steels. *American Society of Mechanical Engineers*, 160, pp. 253–259.
- Smith, G. V., 1971. *Supplemental report on elevated temperature properties of chromium molybdenum steels*. ASTM Data Series, DS 6S1. United States of America: American Society for Testing and Materials.
- Smith, G. V., 1973. *Evaluation of the Elevated Temperature Tensile and Creep Rupture Properties of ½Cr-½Mo, 1Cr-½Mo, and 1¼Cr-½Mo-Si Steels*. ASTM Data Series, DS 50. United States of America: American Society for Testing and Materials.
- Spirax-Sarco, 2011. *The Steam and Condensate Loop*. United Kingdom: Spirax-Sarco Limited.
- Steingress, F. M., 1970. *Low Pressure Boilers*. 1st ed. United States of America: American Technical Society.
- Viswanathan, R., 1993. *Damage Mechanisms and Life Assessment of High-Temperature Components*. Ohio: ASM International.
- Viswanathan, R., Sarver, J. and Tanzosh, J. M., 2006. Boiler Materials for Ultra-Supercritical Coal Power Plants – Steamside Oxidation. *Journal of Materials Engineering and Performance*, 15 (3), pp. 47–51.

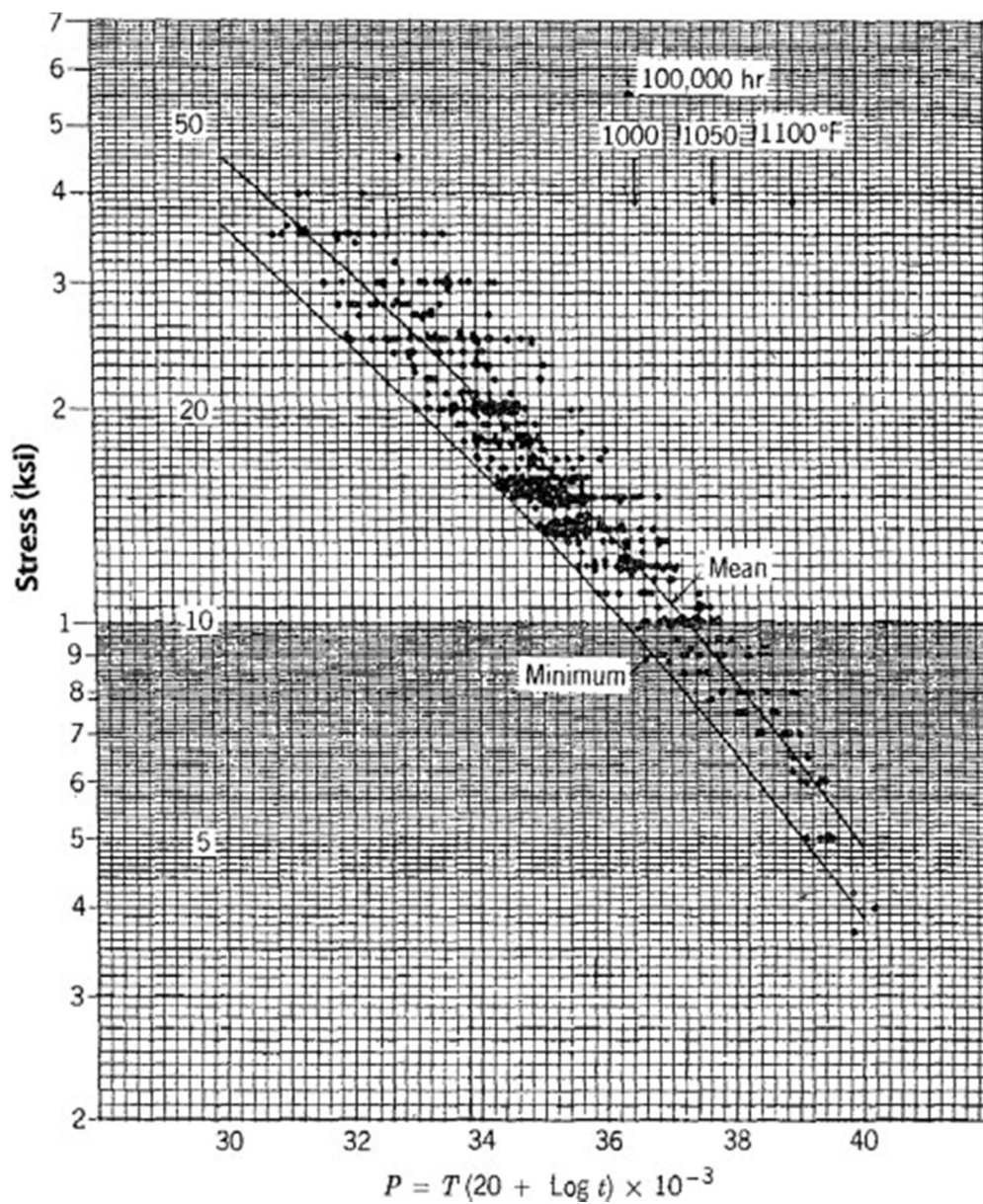
## APPENDICES

## APPENDIX A: Larson-Miller Parameter chart for SA213-T12 (Smith 1973)



Note Conversion: 1 ksi = 6.8946 MPa

**APPENDIX B: Larson-Miller Parameter chart for SA213-T22 (Smith 1971)**



Note Conversion: 1 ksi = 6.8946 MPa

**APPENDIX C: Output results recorded by MATLAB at specified time steps for  
Case B – Performance Analysis on Boiler Tubes**

**\*\* Please refer to the data sheets attached in the next pages \*\***

**Table C.1: List of Variables Used in Appendix C**

<b><u>Variables</u></b>	<b><u>Description [Unit]</u></b>
t_step	= Time step [h]
Tave_o	= Average temperature of oxide-scale [°C]
Tave_m	= Average temperature of metal boiler tube [°C]
hoop	= Hoop stress [MPa]
X1	= Initial scale thickness [mm]
CCDMG	= Cumulative creep damage
thin	= Thinned thickness [m]
Ts0	= Temperature of inner surface of boiler tube [°C]
Ts1	= Temperature of scale/metal interface [°C]
Ts2	= Temperature of outer surface of boiler tube [°C]
HV	= Vickers hardness [HV]
q_flux_0	= Heat flux at inner surface of boiler tube [W/m <sup>2</sup> ]
q_flux_o	= Heat flux at oxide-scale of boiler tube [W/m <sup>2</sup> ]
q_flux_m	= Heat flux at tube metal of boiler tube [W/m <sup>2</sup> ]
q_flux_2	= Heat flux at outer surface of boiler tube [W/m <sup>2</sup> ]
q_flux_ave	= Average of heat fluxes at tube metal and outer surface [W/m <sup>2</sup> ]

**Table C.2: Creep Analysis Results in Time Step (Data Model 1)**

t_step	Tave_o	Tave_m	hoop	X1	CCDMG	thin	Ts0	Ts1	Ts2	HV	q_flux_0	q_flux_o	q_flux_m	q_flux_2	q_flux_ave
1	554.125	555.734	47.3	0	0	0	554.13	554.13	557.34	344.82	34293.19	NaN	34293.19	29567.75	31930.473
250	554.796	557.134	47.3	0.0261	0.001	0	554.05	555.55	558.72	265.04	34098.54	34057.97	34057.97	29399.92	31728.947
500	555.002	557.563	47.3	0.0342	0.001	0	554.02	555.98	559.14	257.3	34038.8	33985.8	33985.8	29348.42	31667.107
1000	555.261	558.103	47.3	0.0444	0.002	0	553.99	556.53	559.68	248.76	33963.7	33895.07	33895.07	29283.67	31589.367
2500	555.707	559.035	47.3	0.0621	0.006	0	553.94	557.48	560.59	236.49	33833.99	33738.37	33738.37	29171.82	31455.098
5000	556.148	559.954	47.3	0.0797	0.012	0	553.88	558.41	561.5	226.67	33706.15	33583.97	33583.97	29061.6	31322.786
10000	556.702	561.111	47.3	0.1021	0.025	0	553.82	559.59	562.64	216.47	33545.3	33389.71	33389.71	28922.92	31156.315
20000	557.4	562.567	47.3	0.1306	0.054	0	553.73	561.07	564.07	205.89	33342.76	33145.17	33145.17	28748.29	30946.73
40000	558.279	564.402	47.3	0.167	0.118	0	553.63	562.93	565.87	194.89	33087.51	32837.06	32837.06	28528.21	30682.636
60000	558.896	565.69	47.3	0.193	0.19	0	553.56	564.24	567.14	188.23	32908.29	32620.77	32620.77	28373.68	30497.226
80000	559.388	566.717	47.3	0.214	0.268	0	553.5	565.28	568.15	183.39	32765.45	32448.44	32448.44	28250.53	30349.482
100000	559.804	567.585	47.3	0.2318	0.351	0	553.45	566.16	569.01	179.55	32644.71	32302.78	32302.78	28146.42	30224.6
120000	560.168	568.344	47.3	0.2476	0.439	0	553.4	566.93	569.76	176.37	32539.06	32175.35	32175.35	28055.33	30115.341
140000	560.494	569.024	47.3	0.2618	0.531	0	553.36	567.62	570.42	173.64	32444.51	32061.31	32061.31	27973.81	30017.556
160000	560.79	569.642	47.3	0.2747	0.628	0	553.33	568.25	571.03	171.25	32358.5	31957.59	31957.59	27899.65	29928.62

**Table C.3: Creep Analysis Results in Time Step (Data Model 2)**

t_step	Tave_o	Tave_m	hoop	X1	CCDMG	thin	Ts0	Ts1	Ts2	HV	q_flux_0	q_flux_o	q_flux_m	q_flux_2	q_flux_ave
1	554.712	556.824	37.57	0	0	0	554.71	554.71	558.94	344.01	35717.09	NaN	35717.09	29628.95	32673.019
250	555.415	558.292	37.57	0.0264	0	0	554.62	556.21	560.38	264.07	35503.4	35460.65	35460.65	29451.69	32456.167
500	555.631	558.743	37.57	0.0346	0.001	0	554.6	556.67	560.82	256.3	35437.77	35381.9	35381.9	29397.24	32389.57
1000	555.903	559.31	37.57	0.0449	0.001	0	554.56	557.24	561.38	247.72	35355.24	35282.87	35282.87	29328.78	32305.827
2500	556.372	560.29	37.57	0.0629	0.003	0	554.5	558.24	562.34	235.4	35212.65	35111.81	35111.81	29210.5	32161.151
5000	556.835	561.256	37.57	0.0808	0.007	0	554.45	559.22	563.29	225.53	35072.09	34943.19	34943.19	29093.89	32018.541
10000	557.417	562.472	37.57	0.1035	0.015	0	554.37	560.46	564.48	215.26	34895.17	34731.01	34731.01	28947.13	31839.066
20000	558.15	564.003	37.57	0.1325	0.032	0	554.28	562.02	565.99	204.59	34672.34	34463.81	34463.81	28762.28	31613.043
40000	559.075	565.934	37.57	0.1697	0.071	0	554.17	563.98	567.88	193.49	34391.42	34127.04	34127.04	28529.24	31328.14
60000	559.724	567.289	37.57	0.1962	0.114	0	554.09	565.36	569.22	186.76	34194.11	33890.56	33890.56	28365.57	31128.066
80000	560.242	568.37	37.57	0.2175	0.162	0	554.02	566.46	570.28	181.85	34036.84	33702.11	33702.11	28235.1	30968.605
100000	560.68	569.284	37.57	0.2357	0.213	0	553.97	567.39	571.17	177.97	33903.87	33542.8	33542.8	28124.8	30833.799
120000	561.062	570.084	37.57	0.2518	0.267	0	553.92	568.21	571.96	174.75	33787.51	33403.41	33403.41	28028.28	30715.843
140000	561.405	570.799	37.57	0.2663	0.324	0	553.87	568.94	572.66	171.98	33683.36	33278.65	33278.65	27941.88	30610.264
160000	561.717	571.45	37.57	0.2796	0.383	0	553.84	569.6	573.3	169.55	33588.61	33165.18	33165.18	27863.28	30514.23

**Table C.4: Creep Analysis Results in Time Step (Data Model 3)**

t_step	Tave_o	Tave_m	hoop	X1	CCDMG	thin	Ts0	Ts1	Ts2	HV	q_flux_0	q_flux_o	q_flux_m	q_flux_2	q_flux_ave
1	567.002	570.077	47.3	0	0	0	567	567	573.15	334.15	65553.2	NaN	65553.2	56520.28	61036.735
250	568.658	573.548	47.3	0.0341	0.002	0	566.79	570.53	576.57	251.27	65028.73	64927.59	64927.59	56068.08	60497.833
500	569.181	574.646	47.3	0.045	0.003	0	566.72	571.65	577.65	242.82	64862.9	64729.81	64729.81	55925.1	60327.454
1000	569.847	576.042	47.3	0.059	0.007	0	566.63	573.06	579.02	233.38	64652.1	64478.43	64478.43	55743.35	60110.891
2500	571.014	578.488	47.3	0.0837	0.02	0	566.48	575.55	581.43	219.55	64282.54	64037.78	64037.78	55424.71	59731.241
5000	572.184	580.941	47.3	0.1088	0.045	0	566.33	578.04	583.84	208.16	63911.92	63595.95	63595.95	55105.16	59350.554
10000	573.685	584.086	47.3	0.1415	0.105	0	566.13	581.24	586.93	195.95	63436.76	63029.62	63029.62	54695.48	58862.549
20000	575.618	588.139	47.3	0.1844	0.258	0	565.88	585.36	590.92	182.77	62824.47	62300.05	62300.05	54167.55	58233.801
40000	578.127	593.398	47.3	0.2414	0.676	0	565.55	590.7	596.09	168.35	62030.02	61353.8	61353.8	53482.58	57418.189
52000	579.266	595.785	47.3	0.2678	0.993	0	565.4	593.13	598.44	162.49	61669.41	60924.42	60924.42	53171.66	57048.037

**Table C.5: Creep Analysis Results in Time Step (Data Model 4)**

<b>t_step</b>	<b>Tave_o</b>	<b>Tave_m</b>	<b>hoop</b>	<b>X1</b>	<b>CCDMG</b>	<b>thin</b>	<b>Ts0</b>	<b>Ts1</b>	<b>Ts2</b>	<b>HV</b>	<b>q_flux_0</b>	<b>q_flux_o</b>	<b>q_flux_m</b>	<b>q_flux_2</b>	<b>q_flux_ave</b>
1	584.802	586.211	47.3	0	0	0	584.8	584.8	587.62	322.14	30014.54	NaN	30014.54	25878.68	27946.607
250	585.622	588.236	47.3	0.0494	0.004	0	584.38	586.86	589.61	238.95	29733.19	29666.24	29666.24	25636.1	27651.169
500	585.88	588.873	47.3	0.0652	0.009	0	584.25	587.51	590.24	230.76	29644.6	29556.6	29556.6	25559.72	27558.16
1000	586.207	589.681	47.3	0.0853	0.018	0	584.08	588.33	591.03	221.68	29532.48	29417.86	29417.86	25463.04	27440.448
2500	586.776	591.085	47.3	0.1208	0.049	0	583.79	589.76	592.41	208.57	29337.41	29176.53	29176.53	25294.85	27235.689
5000	587.339	592.477	47.3	0.1564	0.104	0	583.5	591.18	593.78	197.99	29143.97	28937.3	28937.3	25128.07	27032.687
10000	588.052	594.237	47.3	0.2022	0.226	0	583.14	592.97	595.51	186.89	28899.5	28635.08	28635.08	24917.29	26776.182
20000	588.951	596.46	47.3	0.2614	0.505	0	582.68	595.23	597.69	175.25	28590.69	28253.48	28253.48	24651.03	26452.254
35250	589.86	598.704	47.3	0.3226	0.996	0	582.21	597.51	599.9	165.27	28278.86	27868.37	27868.37	24382.17	26125.267

**Table C.6: Creep Analysis Results in Time Step (Data Model 5)**

t_step	Tave_o	Tave_m	hoop	X1	CCDMG	thin	Ts0	Ts1	Ts2	HV	q_flux_0	q_flux_o	q_flux_m	q_flux_2	q_flux_ave
1	552.013	553.381	47.3	0	0	0	552.01	552.01	554.75	346.57	29164.98	NaN	29164.98	25146.19	27155.585
250	552.569	554.532	47.3	0.025	0	0	551.96	553.18	555.88	267.22	29030.11	28997.07	28997.07	25029.9	27013.483
500	552.739	554.884	47.3	0.0327	0.001	0	551.94	553.54	556.23	259.57	28988.85	28945.7	28945.7	24994.32	26970.01
1000	552.953	555.327	47.3	0.0423	0.002	0	551.92	553.99	556.67	251.14	28937.02	28881.18	28881.18	24949.63	26915.406
2500	553.322	556.09	47.3	0.0592	0.005	0	551.88	554.76	557.42	239.06	28847.58	28769.87	28769.87	24872.52	26821.197
5000	553.685	556.841	47.3	0.0758	0.009	0	551.85	555.52	558.16	229.42	28759.54	28660.31	28660.31	24796.61	26728.458
10000	554.141	557.786	47.3	0.097	0.02	0	551.8	556.48	559.09	219.44	28648.87	28522.6	28522.6	24701.19	26611.896
20000	554.715	558.974	47.3	0.1238	0.042	0	551.74	557.69	560.26	209.14	28509.67	28349.45	28349.45	24581.17	26465.309
40000	555.437	560.469	47.3	0.158	0.092	0	551.67	559.2	561.73	198.49	28334.45	28131.56	28131.56	24430.1	26280.828
60000	555.944	561.517	47.3	0.1822	0.146	0	551.62	560.27	562.77	192.08	28211.56	27978.76	27978.76	24324.14	26151.451
80000	556.348	562.353	47.3	0.2017	0.204	0	551.58	561.12	563.59	187.43	28113.69	27857.11	27857.11	24239.76	26048.434
100000	556.689	563.058	47.3	0.2183	0.264	0	551.55	561.83	564.29	183.76	28031.01	27754.35	27754.35	24168.47	25961.409
120000	556.987	563.675	47.3	0.2329	0.328	0	551.52	562.46	564.89	180.73	27958.69	27664.5	27664.5	24106.12	25885.307
140000	557.253	564.227	47.3	0.246	0.395	0	551.49	563.02	565.44	178.13	27894	27584.12	27584.12	24050.34	25817.226
160000	557.496	564.729	47.3	0.258	0.463	0	551.47	563.53	565.93	175.85	27835.18	27511.04	27511.04	23999.62	25755.329

**Table C.7: Creep Analysis Results in Time Step (Data Model 6)**

t_step	Tave_o	Tave_m	hoop	X1	CCDMG	thin	Ts0	Ts1	Ts2	HV	q_flux_0	q_flux_o	q_flux_m	q_flux_2	q_flux_ave
1	553.947	555.557	54.06	0	0	0	553.95	553.95	557.17	344.95	34318.08	NaN	34318.08	29589.21	31953.645
250	554.617	556.953	54.06	0.026	0.002	0	553.87	555.37	558.54	265.19	34123.86	34083.42	34083.42	29421.75	31752.586
500	554.822	557.382	54.06	0.034	0.004	0	553.84	555.8	558.96	257.46	34064.27	34011.43	34011.43	29370.37	31690.9
1000	555.08	557.92	54.06	0.0442	0.007	0	553.81	556.35	559.49	248.91	33989.35	33920.93	33920.93	29305.78	31613.355
2500	555.526	558.85	54.06	0.0618	0.019	0	553.76	557.29	560.41	236.66	33859.96	33764.64	33764.64	29194.22	31479.433
5000	555.966	559.767	54.06	0.0794	0.039	0	553.71	558.22	561.31	226.84	33732.46	33610.65	33610.65	29084.28	31347.467
10000	556.519	560.92	54.06	0.1016	0.084	0	553.64	559.39	562.45	216.64	33572.02	33416.93	33416.93	28945.95	31181.438
20000	557.216	562.372	54.06	0.13	0.18	0	553.56	560.87	563.88	206.07	33370.01	33173.05	33173.05	28771.78	30972.418
40000	558.093	564.203	54.06	0.1664	0.397	0	553.46	562.73	565.68	195.07	33115.44	32865.8	32865.8	28552.29	30709.043
60000	558.71	565.488	54.06	0.1922	0.637	0	553.39	564.03	566.94	188.42	32936.69	32650.11	32650.11	28398.17	30524.142
80000	559.201	566.512	54.06	0.2131	0.896	0	553.33	565.07	567.95	183.58	32794.24	32478.26	32478.26	28275.35	30376.804
87500	559.364	566.851	54.06	0.22	0.998	0	553.31	565.42	568.28	182.05	32746.97	32421.24	32421.24	28234.59	30327.914

**Table C.8: Creep Analysis Results in Time Step (Data Model 7)**

t_step	Tave_o	Tave_m	hoop	X1	CCDMG	thin	Ts0	Ts1	Ts2	HV	q_flux_0	q_flux_o	q_flux_m	q_flux_2	q_flux_ave
1	554.125	555.734	47.3	0	0	0	554.13	554.13	557.34	344.82	34293.19	NaN	34293.19	29567.75	31930.473
250	554.796	557.134	47.3	0.0261	0.001	0	554.05	555.55	558.72	265.04	34098.52	34057.95	34057.79	29399.92	31728.855
500	555	557.558	47.36	0.0342	0.001	0	554.02	555.98	559.14	257.31	34033.67	33980.67	33939.24	29349.24	31644.241
1000	555.254	558.089	47.47	0.0443	0.002	0.00001	553.98	556.52	559.65	248.77	33948.37	33879.77	33755.44	29286.16	31520.797
2500	555.686	558.992	47.82	0.0621	0.006	0.00004	553.92	557.46	560.53	236.53	33788.35	33692.88	33319.69	29179.44	31249.565
5000	556.101	559.861	48.41	0.0797	0.012	0.00009	553.84	558.36	561.36	226.76	33610.55	33488.74	32700.62	29077.98	30889.301
10000	556.604	560.912	49.64	0.102	0.025	0.00018	553.74	559.47	562.35	216.65	33350.89	33196.28	31578.46	28957.26	30267.86
20000	557.192	562.147	52.3	0.1304	0.053	0.00036	553.57	560.81	563.48	206.27	32953.34	32758.28	29483.27	28819.7	29151.485
40000	557.84	563.514	58.69	0.1666	0.114	0.00072	553.31	562.37	564.66	195.71	32313.78	32069.8	25493.81	28676.52	27085.168
60000	558.214	564.311	67	0.1923	0.181	0.00109	553.08	563.35	565.27	189.5	31754.54	31478.19	21622.7	28601.41	25112.053
80000	558.452	564.828	78.25	0.2128	0.25	0.00145	552.87	564.04	565.62	185.14	31234.16	30933.58	17822.57	28559.55	23191.061
100000	558.606	565.172	94.34	0.2302	0.322	0.00181	552.66	564.55	565.79	181.8	30737.33	30417.58	14076.95	28538.27	21307.607
120000	558.7	565.394	119.3	0.2455	0.395	0.00218	552.46	564.94	565.85	179.12	30256.41	29921.04	10378.3	28531.32	19454.805
140000	558.75	565.524	163.1	0.2591	0.468	0.00254	552.27	565.23	565.82	176.92	29786.9	29438.59	6722.811	28535.08	17628.948
160000	558.763	565.583	260.1	0.2715	0.543	0.0029	552.08	565.45	565.72	175.05	29325.92	28966.78	3108.56	28547.27	15827.913

**Table C.9: Creep Analysis Results in Time Step (Data Model 8)**

t_step	Tave_o	Tave_m	hoop	X1	CCDMG	thin	Ts0	Ts1	Ts2	HV	q_flux_0	q_flux_o	q_flux_m	q_flux_2	q_flux_ave
1	554.127	555.718	47.3	0	0	0	554.13	554.13	557.31	219.31	34297.97	NaN	34297.97	29571.87	31934.922
250	554.798	557.118	47.3	0.0261	0.003	0	554.05	555.55	558.69	170.66	34103.22	34062.64	34062.64	29403.95	31733.299
500	555.004	557.548	47.3	0.0342	0.007	0	554.02	555.99	559.11	165.94	34043.45	33990.44	33990.44	29352.42	31671.43
1000	555.263	558.088	47.3	0.0444	0.013	0	553.99	556.53	559.64	160.73	33968.31	33899.67	33899.67	29287.64	31593.652
2500	555.71	559.021	47.3	0.0621	0.035	0	553.94	557.48	560.56	153.26	33838.53	33742.9	33742.9	29175.74	31459.319
5000	556.15	559.94	47.3	0.0797	0.074	0	553.89	558.42	561.47	147.27	33710.63	33588.42	33588.42	29065.46	31326.943
10000	556.704	561.097	47.3	0.1021	0.156	0	553.82	559.59	562.6	141.05	33549.69	33394.08	33394.08	28926.7	31160.392
20000	557.402	562.553	47.3	0.1306	0.337	0	553.74	561.07	564.04	134.6	33347.05	33149.43	33149.43	28751.99	30950.708
40000	558.281	564.389	47.3	0.167	0.741	0	553.63	562.93	565.85	127.89	33091.67	32841.18	32841.18	28531.8	30686.488
51750	558.664	565.187	47.3	0.1831	0.999	0	553.59	563.74	566.63	125.32	32980.62	32707.17	32707.17	28436.05	30571.605

**OVERALL SUMMARY:**

Model 1 in critical state at 0 hours due to hoop stress exceeds max allowable stress.

Model 5 in critical state at 0 hours due to hoop stress exceeds max allowable stress.

Model 2 in critical state at 97750 hours due to hoop stress exceeds max allowable stress.

Model 6 fails at 87500 hours due to creep damage.

Model 3 fails at 52000 hours due to creep damage.

Model 7 in critical state at 0 hours due to hoop stress exceeds max allowable stress.

Model 4 fails at 35250 hours due to creep damage.

Model 8 fails at 51750 hours due to creep damage.

### APPENDIX D: Sample Calculation on Minimum Tube Wall Thickness

By referring to Appendix C, at 1<sup>st</sup> hour for Model 7, the MATLAB had recorded tube metal average temperature,

$$T_{ave\_m} = 555.734 \text{ } ^\circ\text{C}$$

Use  $T_{ave\_m}$  to conduct simple table interpolate for maximum allowable stress,  $S$  for T22 grade in Table 2.3.

$$S = \left[ \frac{555.734 - 550}{575 - 550} \times (34.5 - 47.7) \right] + 47.7 = 44.672 \text{ MPa} = 6478.9 \text{ psi}$$

Assume tube is a strength welded type;

$$e = 0$$

Tube outer tube diameter and the operational pressure are obtained from Table 3.5;

$$D = 0.0508 \text{ m} = 2 \text{ in}$$

$$P = 7 \text{ MPa} = 1015.23 \text{ psi}$$

From Equation 2.3;

$$t = \frac{PD}{2S + P} + 0.005D + e$$

$$t = \frac{1015.23 \times 2}{(2 \times 6478.9) + 1015.23} + 0.005(2) + 0$$

$$t = 0.1553 \text{ in} = 0.003945 \text{ m}$$

$$t = 3.945 \text{ mm}$$